CAF variants control the tumor-immune microenvironment and predict skin cancer malignancy

Agnes Forsthuber[1], Ana Korosec[1,*], Tina Jacob[2,*], Bertram Aschenbrenner[1], Karl Annusver[2], Sophie Frech[1], Kim Purkhauser[1], Natalia Krajic[1], Katharina Lipp[1], Franziska Werner[3], Vy Nguyen[3], Johannes Griss[3], Wolfgang Bauer[3], Ana Soler Cardona[3], Benedikt Weber[1], Wolfgang Weninger[3], Bernhard Gesslbauer[4], Clement Staud[4], Jakob Nedomansky[4], Christine Radtke[4], Stephan N. Wagner[3], Peter Petzelbauer[1], Maria Kasper[2,#] and Beate M. Lichtenberger[1,#]

Affiliations:
[1]Skin and Endothelium Research Division, Department of Dermatology, Medical University of Vienna, Austria
[2]Department of Cell and Molecular Biology, Karolinska Institutet, Sweden
[3]Department of Dermatology, Medical University of Vienna, Austria
[4]Division of Plastic and Reconstructive Surgery, Department of Surgery, Medical University of Vienna, Austria
* equal contribution
# equal contribution

Corresponding authors:
beate.lichtenberger@meduniwien.ac.at
maria.kasper@ki.se

Running title: CAF variants shape the tumor-immune microenvironment

Keywords: cancer-associated fibroblasts; skin cancer; single-cell RNA sequencing; tumor microenvironment; basal cell carcinoma; squamous cell carcinoma; melanoma

Abstract:
Cancer-associated fibroblasts (CAFs) play a key role in cancer progression and treatment outcome. Here, we elucidate the yet unresolved intra-tumoral CAF variety in three skin cancer types at molecular and spatial single-cell resolution in a large cohort. We show that two out of three CAF subtypes contribute to tumor immune surveillance with distinct mechanisms. Matrix CAFs (mCAFs), a previously unknown subtype present in early-stage tumors, ensheath tumor nests and synthesize extracellular-matrix to prevent T cell invasion. Immuno CAFs (iCAFs), which express proinflammatory and immunomodulatory factors, are only detected in high abundance in aggressive tumors. Strikingly, iCAFs but not tumor cells are the exclusive celltype producing chemokines and, thus, play a key role in immune cell recruitment and activation. Mechanistically, we show that cancer cells transform adjacent healthy fibroblasts into cytokine-expressing iCAFs, which subsequently recruit immune cells and modulate the immune response. In conclusion, targeting CAF variants holds promise for improved efficacy of immunotherapy.

Statement of significance:
While it is accepted that fibroblasts affect cancer progression, the underlying molecular programs remain unclear. We unravel a multi-step cascade demonstrating that tumor cells transform healthy fibroblasts into CAFs, which critically impact immune surveillance via iCAFs being the exclusive source of chemokines and mCAFs promoting T cell exclusion.

Introduction:
Underestimated for a long period of time, fibroblast plasticity and the function of distinct fibroblast subsets in tissue homeostasis and disease has only become a major scope of research in the past decade. In cancer, fibroblasts have been established as a key component of the tumor microenvironment (TME) affecting both cancer progression and the response to therapies. Fibroblast heterogeneity has been acknowledged previously as playing both tumor suppressive as well as tumor supportive roles [1–7]. Recent studies even demonstrated that also mutations in fibroblasts can lead to cancer (reviewed in Lichtenberger and Kasper, 2021)[8], further highlighting their impact on tumorigenesis. It also has become clear that in a single tumor several fibroblast subtypes exist in parallel with different functions [9]. Single-cell RNA sequencing (scRNA-seq) has revealed manifold dermal fibroblast subpopulations in mouse and human healthy skin [10–12]. Likewise, fibroblast heterogeneity has been studied in many cancers such as breast cancer [13], pancreatic ductal adeno carcinoma [14,15], colorectal cancer [16,17], head and neck squamous cell carcinoma [18] and many more [19]. Comparable single-cell transcriptomics studies in skin cancer are missing. The few previous scRNA-seq based studies

of human melanoma, basal cell carcinoma (BCC) and cutaneous squamous cell carcinoma (SCC) mainly focused on tumor infiltrating lymphocytes, thus these datasets included only a few or no fibroblasts [20–25]. In the past years, scRNA-seq revealed a range of different cancer-associated fibroblast (CAF) subsets with newly described markers in various tissues. Besides context-dependent and/or uniquely described CAF subsets in certain types of cancer [26–28], a common trait among many of these studies is the presence of a CAF subtype with immunomodulating characteristics, secreting IL6 and other proinflammatory cytokines, and a CAF subtype with a myofibroblastic phenotype defined by its widely accepted signature molecule alpha smooth muscle actin (ACTA2) [13,29–34].
In healthy skin, lineage tracing mouse models and functional studies in mouse and human skin identified two major fibroblast subsets, the papillary fibroblasts in the upper dermis and the reticular fibroblasts of the lower dermis. They exhibit distinct roles during development, ECM deposition, wound healing and differ in their potential to differentiate into adipocytes [35–38]. Whether these two subpopulations evolve into CAFs, or impact skin tumor progression differently, is still an unresolved topic. So far, all studies on skin CAFs focused on CAFs as a unit, their overall marker gene expression, capability to stimulate migration of tumor cells, secretion of soluble mediators, and their response to anti-tumor therapies [39–41], leaving a major gap in knowledge about the presence of CAF subtypes, their association with tumor malignancy and different functional roles, which we address in this study.

Here, we investigated the cellular ecosystem of BCC, SCC and melanoma – with emphasis on fibroblast heterogeneity – using the sensitive Smart-seq2 scRNA-seq platform (n=10 tumors) and mRNA staining *in situ* (n=35 tumors). SCCs vary from highly to poorly differentiated with increasing metastatic potential [42] and BCCs, which metastasize very rarely, are primarily tissue-destructive locally [43]. Both cancer types arise from keratinocytes. In contrast, melanoma is a skin cancer type derived from melanocytes that comes with a high potential of metastatic spread and poor survival rates [44]. The unique combination of these three different types of skin tumors in one dataset allowed us to dissect similarities and differences between those cancer types with a special focus on the fibroblast heterogeneity in a healthy skin, premalignant and cancer context. Collectively, our work deconstructed CAF heterogeneity in skin cancer, which led to important new insights. We reveal a previously unrecognized CAF subtype – the mCAF – which likely plays a role in T cell marginalization, and propose that the iCAF subtype is an important regulator of immune cell recruitment and immune surveillance.

Results:

A collective single-cell atlas of primary BCC, SCC and melanoma to deconstruct skin cancer

To explore fibroblast heterogeneity and their cross talk to tumor and immune cells, we collected biopsies from four cutaneous squamous cell carcinomas (SCCs), three basal cell carcinomas (BCCs), three melanomas and biopsies of sun-protected skin from five healthy

donors (Supplementary table 1). For the tumor samples, fresh 4 mm punch biopsies from the tumor center and from the non-lesional adjacent skin were collected directly after surgery. Upon dissociation of the tissues, the samples were enriched for keratinocytes, fibroblasts and immune cells by FACS (Figure S1A and S1B) and the cells were directly sorted into 384-well plates for sequencing with the sensitive Smart-seq2 technology (Figure 1A). In two healthy control samples a random live-cell sorting approach was used, explaining why keratinocytes are underrepresented in these samples (Healthy I, Healthy II, Figure 2A), which was compensated by a separate keratinocyte enrichment protocol in healthy samples Healthy III-V (Figure S1A and 2A). In total, 5760 cells were sequenced, finally retaining 4824 cells at a median depth of 486146 RPKM/cell and a median of 3242 genes/cell after quality control and filtering (Figure S1C). Unsupervised clustering separated cells into fibroblasts, healthy and malignant keratinocytes as well as melanocytes, immune cells, and endothelial cells (Figure 1B). Assignment of cell type identity was based on commonly accepted signature gene expression: *COL1A1* and *PDGFRA* for fibroblasts, *RERGL* for vascular smooth muscle cells (vSMC), *KRT5*, *KRT14* and *CDH1* for keratinocytes, *CD45* for immune cells, *TYR*, *MITF* and *MLANA* for melanocytic cells and *CDH5* for endothelial cells (Figure 1B and 1C).

Tumor cells express a range of additional keratins

Second-level clustering of healthy and neoplastic keratinocytes resulted in a clearly separated cluster of healthy keratinocytes (hKC) with basal (*KRT5*, *KRT14*, *COL17A1*) and differentiating/suprabasal (*KRT1*, *KRT10*) marker gene expression. The majority of cells in clusters KC1–KC5 contained tumor cells from BCC and SCC samples, with tumor cells expressing a range of additional keratins that are not expressed by healthy skin keratinocytes (Figure 2A and Supplementary table 2). For example, BCC cells expressed *KRT5*, *KRT14* and additionally *KRT17* [45], which are foremost clustering in KC2 and KC3. As expected for the Hedgehog(Hh)-pathway-dependent BCC, we confirmed *PTCH1/2* overexpression in clusters KC2 and KC3 (Figure 2A and S2B) [46]. Cells from the SCC samples clustered in KC1, KC2, KC4 and KC5. KC1 – which primarily comprised cells of donor sample SCC III (Figure 2A and S2C) – expressed in addition to *KRT5*, *KRT14*, and *KRT17* the typical SCC keratins like *KRT6A* and *KRT16,* and showed reduced expression of *KRT1* and *KRT10* [45] (Figure 2A). Cells from donor sample SCC IV, a Bowen carcinoma (SCC *in situ*) (Supplementary table 1), mainly clustered in KC2, KC4, and KC5 that showed reduced expression of *KRT1*, *KRT10*. KC2 and KC5 also displayed neo-expression of *KRT16* and *KRT19,* respectively, which has been previously described for this SCC subtype [45] (Figure 2A). Notably, KRT7, KRT18 and KRT19 were only expressed by KC1 and KC5, which were primarily represented by cells originating from SCC samples (Figure 2A). It has been shown that tumors co-opt developmental programs for their progression [1]. In our dataset we find previously described keratins of the simple skin epithelium of the first trimester embryo such as KRT18 and KRT19 expressed in SCC cluster KC1 and KC5, or KRT8 expressed in BCC cluster KC2 [47]. Interestingly, in KC4, cells from BCC, SCC, melanoma as well as healthy skin clustered together, but did not express any of the classical keratinocyte markers (Figure 2A and S2C).

The tumor microenvironment strongly impacts non-malignant cell types

Second-level clustering of melanocytes and melanoma cells revealed one cluster of healthy melanocytes (hMC) derived from healthy skin samples, and one separate cluster of non-malignant melanocytes derived mainly from SCC and BCC samples (tumor melanocytes, tMC). This separate clustering can likely be explained by the influence of the TME on the expression pattern of melanocytes in comparison to melanocytes from healthy skin. The melanoma samples separated into four different donor-specific clusters: MEL1 and MEL2 coming from Melanoma I, MEL3 from Melanoma II, and MEL4 from Melanoma III (Figure 2B and Supplementary table 2). In order to explain this donor-specific clustering, as well as to segregate malignant from non-malignant cells, we inferred copy number variation (CNV) analysis on our scRNA-seq data using the R package *inferCNV* [18,24]. We performed CNV analysis for all cells from each tumor sample and estimated the malignancy for each individual cell in comparison to all cell types from healthy skin, as previously described [18] (Figure 2C and S2A). Melanoma cells, which are known for their high mutational load [48], displayed strong CNV patterns. Remarkably, these patterns were donor-specific despite of sharing the same histological subtype (acral lentiginous melanoma, ALM) and body location (heal/toe) (Supplementary table 1). Also, keratinocytes of SCCs can display CNVs dependent on their malignancy grade. In our data, SCC III (forming cluster KC1) shows CNVs in chromosomes 4, 13 and 14, which matched well with its histopathological characterization of a poorly differentiated, aggressive type of SCC (Supplementary table 1). The remaining BCC and SCC samples did not display unique CNV patterns, thus for BCC samples we additionally utilized high *PTCH1* and *PTCH2* expression (*PTCH1/2 high)* in comparison with healthy skin samples to pinpoint tumor cells (Figure S2B). As the non-malignant cells mixed across almost all donor samples, such as tMC or immune cells (Figure 2B-C), we did not regress for donor differences; thus, donor-specific tumor cell clustering in KC1 and MEL1–MEL4 is likely the result of genomic aberrations and not an effect of batch variations.

Subclustering of immune cells resulted in eight immune cell clusters, including T and B cells, granulocytes and antigen presenting cells (Figure 2D and Supplementary table 2). Interestingly, CD4 and CD8 T cells from healthy samples (hTcells) formed a distinct cluster, adjacent to CD4 (tCD4) and CD8 T cells (tCD8) from tumor samples (Figure 2D and S2C). This can be explained by a different activation status of T cells in healthy or tumor samples: Increased expression of granzymes, perforin and *IFNγ* indicated T cell activation in CD8 T cells from tumor samples versus healthy tissue (Figure 2E). Regulatory T cells (Tregs), *CD4$^+$IL2RA$^+$FOXP3$^+$*, were found mixed with CD4 T cells from tumor samples (tCD4) (Figure 2D, 2E and S2C).

Fibroblasts from healthy skin cluster separately from CAFs

Second-level clustering of fibroblasts and vSMCs (2239 cells) resulted in 7 subclusters: two main clusters from healthy skin samples (papillary fibroblasts (pFIB), reticular fibroblasts

(rFIB)), four CAF subclusters (matrix CAFs (mCAF), immuno CAFs (iCAF), *RGS5*$^{+}$ CAFs and pericytes (*RGS5*$^{+}$ cells), unclassifiable CAFs (ucCAF)), and one vSMC cluster (Figure 3A, S3A and S3B). We used differentially expressed genes as well as commonly accepted markers to define these subclusters. Reassuringly, fibroblasts from the tumor-adjacent skin samples were found on the transition between healthy and tumor samples, and within the *RGS5*$^{+}$ as well as vSMC cluster (Figure S3A), indicating that CAFs may develop from skin-resident fibroblasts (pointing towards field cancerization) [49].

Importantly, established markers for papillary and reticular fibroblasts could be assigned to the two subclusters comprising cells from healthy donors. *COL6A5*, *COL23A1* and *HSPB3* [10], the Wnt inhibitors *APCDD1* and *WIF1* [10,50], *NTN1* and *PDPN* [51] are commonly accepted markers for papillary fibroblasts and were found to be expressed in the pFIB cluster. *DPP4* (*CD26*), which was described as a marker for papillary fibroblasts by Tabib et al. 2018, was expressed in both subpopulations in our data (Figure S3C), as shown by Korosec et al., 2019 and Vorstandlechner et al., 2020 [12,37]. The healthy fibroblast subcluster rFIB expressed genes that are characteristic for reticular fibroblasts: *THY1* [37], *FMO1*, *MYOC* and *LSP1* [11], *MGP* and *ACTA2* [51] as well as the preadipocyte marker genes *PPARG* and *CD36* [37] (Figure S3C). Thus, we conclude that the healthy fibroblast cluster pFIB represents papillary fibroblasts, and rFIB represents reticular fibroblasts (Figure 3A, 3B and S3C).

Different skin cancer types comprise both common and tumor type-specific CAF subsets

Subclustering segregated four CAF populations: mCAFs, iCAFs, *RGS5*$^{+}$ cells, and ucCAFs. Matrix CAFs (mCAFs) exhibited increased expression of extracellular matrix components such as collagens (*COL1A1*, *COL1A2*, *COL3A1)*, Lumican (*LUM*), Periostin (*POSTN*) or Tenascin-C (*TNC*) compared to all other fibroblast clusters (Figure 3A, 3B and Supplementary table 2). Immuno CAFs (iCAFs) presented with enhanced expression of the matrix remodelers *MMP1* and *MMP3*, the pro-inflammatory cytokines *IL6* and *CXCL8* and the immune-suppressive molecule *IDO1* among their top ten differentially expressed genes (DEGs), thus suggesting an immunoregulatory and cancer invasion-supportive phenotype (Figure 3A and 3B). Intriguingly, the mCAF cluster harbored fibroblasts from all BCC and from highly differentiated SCC samples (mainly SCC I and SCC IV), whereas the iCAF cluster contained fibroblasts from all melanoma samples, one poorly differentiated SCC (SCC III) and one BCC (BCC II). While the presence of these subsets seems to depend on the skin cancer type with iCAFs being associated with the most aggressive tumors, *RGS5*$^{+}$ cells were found in all tumor samples independently of skin cancer type and malignancy (Figure 3A, S3A and S3B).

Since *RGS5*$^{+}$ cells express the key signature molecule *ACTA2* (in combination with *COL1A1*, Figure 4A), this subset likely represents activated fibroblasts that are usually termed myofibroblasts in wounded or fibrotic tissues [52], or myoCAFs in different cancer types [33]. However, they also express genes among their top DEGs that have been used as pericyte markers, such as *RGS5*, *KCNJ8, ACTA2* and *MCAM* (Figure 3B) [53–55]. *RGS5*$^{+}$ cells also share some

markers with the vSMC cluster, such as *ACTA2*, *TAGLN* and *MCAM*, which are markers for perivascular cells in various tissues [37,56]. The vSMC population formed its separate cluster and was clearly defined by *RERGL*, *MYH11*, *CNN1* in addition to *ACTA2* [54] (Figure 3A and 3B). Unclassifiable CAFs (ucCAFs) represent a minor population with an inconclusive gene expression pattern and mixed cell contribution from almost all tumor samples, which we therefore did not consider further for in-depth discussion (Figure 3A and 3B).

$ACTA2^+$ and FAP^+ in combination identifies all CAF subpopulations in skin tumor samples

Previous studies have used different single markers like ACTA2 or FAP to identify or isolate CAFs in different tissues [57]. However, a query on previously described CAF marker genes showed that, in our dataset, most of them are either restricted to a distinct CAF subset, or found in all fibroblast clusters including healthy fibroblasts, but do not solely identify all CAF subsets (Figure S3D). A good strategy to detect all CAFs within skin tumor samples is combining the two most frequently used CAF markers *ACTA2* and *FAP*. Although this combination also includes vSMCs, it allows to enrich for all CAF subpopulations populations when used together (Figure S3D).

The $RGS5^+$ cells are best described as a mixed population of myoCAFs and pericytes

When we investigated the detailed gene expression profiles of the distinct CAF subtypes we suspected that the $RGS5^+$ cluster likely comprises both myoCAFs and pericytes, therefore we chose the neutral term "$RGS5^+$ cells" for this cluster. In detail, $RGS5^+$ cells expressed *ACTA2* – the signature gene for myofibroblasts and myoCAFs – in combination with *COL1A1*. The expression of *PDGFRB*, *TAGLN*, *RGS5*, *DES* and the absence of *PDGFRA* suggests that this cluster also comprises pericytes [53–55] (Figure 4A). Interestingly, the $RGS5^+$ cluster also shows expression of *NOTCH3*, *EPAS1*, *COL18A1* and *NR2F2*, markers that were used to describe so-called vascular CAFs (vCAFs), a CAF subset defined by Bartoschek et al., 2018 in a mouse model for breast cancer [58] (Figure S4A). Of note, endothelial markers such as *CDH5*, *PECAM1*, *TIE1* or *CD62* were not expressed in the $RGS5^+$ cluster (Figure S4B).

To characterize the nature of the $RGS5^+$ cluster further, we stained tumor sections for Transgelin (TAGLN), which is a prominently expressed gene in this cluster. This tissue staining revealed TAGLN protein along blood vessels as expected, but also within the tumor stroma without direct contact to vessel-like structures (Figure 4A). Protein expression of Desmin (DES), a marker for pericytes and vSMCs [52,53] was restricted to vessels (Figure 4A). *DES* was only expressed by few cells on RNA level, which was not sufficient to identify a separate pericyte cluster within the $RGS5^+$ cells in our sequencing data set [59,60]. Next, we performed mRNA co-staining for *RGS5, COL1A1* and *PDGFRA* mRNA to validate our sequencing data and to verify the stromal and perivascular presence of $RGS5^+$ cells (Figure 4B, Figure S4C). In tumor regions (Figure 4B region 1-3 and S5C region 1-2), a positive staining for *RGS5* was detected both at vessel-structures and within the stroma, in comparison to the peritumoral area, where *RGS5* staining was only found surrounding vessel-like structures (Figure 4B, region 4).

However, staining intensity was stronger in perivascular cells compared to stromal *RGS5*$^{+}$ cells in the tumor tissue, which was not reflected in the scRNA-seq data. The expression of *PDGFRA* was generally weak, both in adjacent skin and tumor tissue (Figure 4B).

To shed light on the discrepant classification of cells as being myofibroblast-like CAFs or pericytes in tumor samples, we reanalyzed a publicly available head and neck squamous cell carcinoma (HNSCC) data set [18] and put it in comparison with our dataset. Puram et al. classified the tumor fibroblasts into CAFs, myofibroblasts and intermediate (resting) fibroblasts. We extended their published marker gene set by commonly accepted pericyte markers and found those enriched in the myofibroblast cluster only, revealing a very similar expression profile to our *RGS5*$^{+}$ cell cluster (Figure 4C). The fact that this formerly defined myofibroblasts have been defined as pericytes upon reanalysis by another group [61], suggests that myofibroblasts and pericytes share a very close gene expression pattern which indeed does not allow segregation by transcriptional profiling. Thus, the absence of histological stainings in previously published datasets impeded an accurate definition of those cells, and only the combination of histological localization and gene expression allows proper lineage designation. We conclude that the *RGS5*$^{+}$ cell cluster within our as well as the HNSCC dataset comprises both pericytes and CAFs.

In situ validation and spatial localization of mCAF and iCAF subsets

We verified the presence of iCAFs and mCAFs by mRNA staining *in situ* in the same tumor samples that were sequenced as well as in additional 29 independent tumor biopsies (n=39 tumors in total). We used *COL11A1* and *PTGDS* as markers for mCAFs, and *MMP1* as a marker for iCAFs, in co-stainings with the pan-fibroblast marker *COL1A1* (Figure 5A and 5B). mCAFs were found abundantly in large patches ensheathing tumor-cell nests and at the tumor-stroma border of BCC and SCC (Figure S5A and S5B). Interestingly, the Bowen carcinoma, SCC IV, showed strong *COL1A1*$^{+}$*COL11A1*$^{+}$ expression in the infiltrative tumor part, whereas less intense staining was seen in the exophytic/papillomatous tumor part, and no staining (apart from vessel-like structures) was seen in the unaffected adjacent skin (Figure S5B).
iCAFs were present in lower numbers, intermingled between *MMP1*$^{-}$*COL1A1*$^{+}$ cells intratumorally in stromal nests and strands that pervade the tumors (Figure S5C and S5D).

mCAFs form a barrier around tumor nests

We investigated the expression of matrix-associated genes (collagens, laminins, lysyloxidases and other ECM genes) and immune response or cancer invasion-associated genes (MMPs, chemokines, interleukins and immunomodulatory genes) by module scores and found a significant enrichment of matrix-associated genes in mCAFs and immuno/invasiveness-associated genes in iCAFs (Figure S6A, S6B and Supplementary table 3). Additionally, we interrogated for possible ligand-receptor interactions: mCAFs exhibit a strong expression of collagens and other ECM genes, whose receptors are found on healthy and neoplastic keratinocytes and melanocytes as well as on immune cells (Figure 5C). COL11A1 protein

staining revealed a dense network of collagen fibers aligning the basement membrane of tumor nests (Figure S5E), indicating that mCAFs may control T cell marginalization as has been shown for COL11A1 expressing CAFs in lung cancer [62].

iCAFs are the major source of cytokines in the TME

iCAFs strongly express immunomodulatory genes, including *TGFB3* and *LGALS9*, proinflammatory cytokines such as *IL1B* and *IL6*, and are an exclusive source of many chemokines (Figure 5D). Notably, iCAFs from melanoma samples express high levels of *CXCL1-8* but not *CXCL9-13*, whereas the expression of *CXCL9-13* is high in iCAFs of the SCC IV and BCC sample. Only *CXCL2* is equally high expressed in iCAFs from all tumor samples. Similarly, *IL1B* is expressed at much higher levels in iCAFs derived from melanoma, while *TGFB3* and *LGALS9* are strongly expressed in iCAFs from BCC and SCC but not melanoma (Figure 5D). We confirmed the CAF-derived expression of several cytokines including *CXCL2*, *CXCL8* and *IL24* by mRNA staining *in situ* (Figure 6A). Furthermore, quantification of cytokine-expressing iCAFs in tumor sections revealed that non-invasive tumors (nodular BCC, highly differentiated SCC and superficially spreading melanoma) barely harbored iCAFs, whereas undifferentiated SCC and nodular melanoma as well as infiltrative BCC presented with large clusters of iCAFs (Figure 6B), which confirms the transcriptomic data (Figure 3A). Furthermore, we confirmed that CAFs are a major source for cytokines in the TME in an entirely independent single cell transcriptomics dataset of melanoma (n=5) (Figure S6C). These samples express exceptionally high levels of CCL2, CXCL12 and CXCL14. Along these lines, also CAFs from oral SCCs display stronger cytokine expression than their respective tumor cells (Figure S6D).

These results led us to hypothesize that the cancer cells of invasive cancers (but not from non-invasive ones) may directly impact the phenotype of tumor-adjacent fibroblasts. To test this, we isolated primary dermal fibroblasts from healthy skin (NHDF) and treated them with conditioned medium collected from melanoma and SCC cell lines. Intriguingly, the conditioned medium of cultured cell lines derived from melanoma metastases (VM08 and VM15[63]) or from a highly aggressive SCC (SCC13[64]) strongly induced the expression of different cytokines and chemokines in healthy-skin fibroblasts and resulted in a proliferative and activated iCAF-like phenotype *in vitro* (Figure 6C). On the contrary, VM19, which was derived from a primary melanoma, did not induce cytokine expression. Thus, we conclude that the secretome of invasive tumor cell lines can transform normal fibroblasts into iCAF-like cells *in vitro*.

Taken together, *in situ* stainings of the marker genes identified in our scRNAseq screen confirmed that mCAFs are primarily found in benign tumors, while the presence of iCAFs correlated with malignant progression (Figure 6B and 6D). Importantly, receptor-ligand analysis revealed that iCAFs, which are associated with the most aggressive tumors, express many immunomodulatory factors that bind to receptors expressed primarily on T cells and NK cells. Notably, the heat map in Figure 5D shows that the majority of cytokines and chemokines are expressed by fibroblasts and not by tumor cells, indicating that not the tumor

cells but the stromal cells (fibroblasts) are key players in immune cell recruitment and activation. Furthermore, since mCAFs ensheath tumor nests and synthesize large amounts of ECM proteins, it is likely that they are involved in T cell exclusion (Figure 6D).

Discussion:

Fibroblasts are important contributors to the TME. They can exert pro- as well as anti-tumorigenic functions by stimulating tumor cell survival and proliferation, modifying ECM stiffness, supporting metastasis, influencing therapy response, regulating immune cell recruitment via chemokine secretion and inflammatory responses [34,65]. Inter- and intratumoral CAF heterogeneity have been appreciated ever since scRNA-seq methods have become available. However, their different functions in the TME remain largely inexplicit. The scRNA-seq based works that have been published for skin cancers, four melanoma studies [20,22–24], one SCC study [21] and one study containing BCCs and SCCs [25], either only contained a very small number of fibroblasts or fibroblast heterogeneity was not the focus of the analysis. Considering the large knowledge about fibroblast diversity in healthy human dermis [10–12,37], a screen on the CAF heterogeneity in human skin tumors was required to fill the missing gap, which we achieved with the present work.

We have previously shown that healthy human skin comprises two functionally distinct fibroblast subsets (papillary and reticular fibroblasts) which can be distinguished by the expression of *CD90* (*THY1*) [37]. The present scRNA-seq screen confirmed that *CD90*, which is still frequently used as the sole fibroblast marker to isolate or visualize skin fibroblasts, is only expressed by the reticular subpopulation (Figure S3C). Although the majority of CAFs express *CD90* (Figure S3C), our data do not allow to conclude whether CAFs develop only from skin-resident reticular fibroblasts or whether they acquire expression of *CD90* upon activation.

Of note, the RNA expression level of *FAP* in the scRNA-seq data does not reflect the FAP protein expression on the fibroblasts entirely, as we used FAP and CD90 surface expression to enrich for fibroblasts by FACS (Figure S1B and S3C).

In the skin cancer samples, we identified three distinct fibroblast populations (excluding the small population of ucCAFs). Immuno CAFs (iCAFs) show a characteristic expression of proinflammatory cytokines (*IL1B*, *IL6*), chemokines (CXCR2 ligands) and immunomodulating molecules (*IDO1*) and thus seem to be analogue to the previously described iCAFs in other cancer types (Figures 3B and 5D) [33]. Matrix CAFs (mCAFs), which we identified as a new separate CAF population, are not to be confused with myofibroblasts described in other publications[33]. mCAFs exhibit increased matrix production but without the expression of *ACTA2* and myosin light chain proteins (Figures 3B and 5C).

Most interestingly, in our dataset iCAFs and mCAFs seem to be mutually exclusive and can likely be attributed to skin cancer types with higher (iCAFs) and lower (mCAFs) metastatic potential. The only exception were fibroblasts from BCC II, which were found in the iCAF cluster even though BCC II is histologically not different to the other two BCC samples (Supplementary Figure 3). *In situ* localization in more than 30 tumor samples confirmed that

iCAFs are present in aggressive tumors with strong stromal contribution (Figure 5, 6D and S5C-D).

The *RGS5*$^+$ cluster contains cells from all samples, including healthy controls. According to differential gene expression, the *RGS5*$^+$ cluster would commonly be termed as myofibroblasts/myoCAFs due to the characteristic expression of *ACTA2*, *MYH11* and *COL1A1*. However, the *RGS5*$^+$ cluster also showed a marker profile that can be attributed to pericytes (*RGS5*, *PDGFRB*, *KCNJ8*, *TAGLN, MCAM*) (Figure 3B and 4A). We demonstrate by *in situ* immunohistochemistry that *RGS5*$^+$ cells are not only found in a perivascular localization but are also distributed throughout the stroma in tumor regions. In contrast, in unaffected skin, *RGS5*$^+$ cells are restricted to a perivascular localization (Figure 4A and 4B). Thus, an exclusive definition as myofibroblasts/myoCAFs or pericytes for this cluster seems to be inappropriate. The impossibility to discern myofibroblasts/myoCAFs from pericytes on RNA level has been a general issue, as we found very similar expression patterns of the myofibroblasts/pericytes in a HNSCC dataset, once defined as myofibroblasts [18], and once defined as pericytes [61] (Figure 5C). It has been suggested that pericytes are able to leave the vessel wall and contribute to the tumor stroma in a process called pericyte-fibroblast transition (PFT) [66]. To our knowledge, PFT has not been shown in skin cancer. A recent pan-cancer scRNA-seq study suggested that a small CAF subset arose from endothelial cells. However, this was concluded from transcriptional data but not confirmed *in situ* [67]. Whether *RGS5*$^+$ CAFs originate from pericytes or skin-resident fibroblasts cannot be concluded from this study. It is of higher importance that *RGS5*$^+$ *ACTA2*$^+$ CAFs are present in all tumor samples, which might represent a general phenotype that is similar to activated fibroblasts expressing *ACTA2* in non-cancerous conditions, such as wound healing [68,69]. Notably, Grout et al. recently described an MYH11$^+$aSMA$^+$(ACTA2$^+$) and COL4A1 expressing CAF subset in non-small cell lung cancer that might be involved in T cell exclusion. The *RGS5*$^+$ CAFs in our study (which we appointed a T cell-exclusion role from tumor nests) also expressed *MYH11*, *ACTA2* and *COL4A1*[62].
CAFs share common features with fibroblastic reticular cells (FRCs) within lymph nodes, which generate ECM conduits to guide the traffic of immune cells and the transit of potential antigens [70]. It is established that CAFs participate in T-cell exclusion from tumor nests [71]. Several studies have reported reduced T cell infiltration in CAF-rich tumors compared to their CAF-low counterparts [72]. mCAFs are detected at the tumor-stroma interface and ensheath tumor nests. As they synthesize a range of ECM proteins including COL11A1, which we detected as dense fibers surrounding tumor nests, we propose that mCAFs play a crucial role in T cell marginalization. A similar function was described for a subset of FAP$^+$aSMA$^+$ lung CAFs expressing COL11A1/COL12A1 or COL4A1 in human lung cancer [62]. Thus, targeting mCAFs may improve the efficacy of immunotherapy in patients bearing T cell-excluded tumors. Indeed, a whole tumor cell vaccine genetically modified to express FAP significantly reduced cancer growth in a murine model of lung cancer and melanoma by directly inhibiting CAFs and simultaneously enhancing T cell infiltration [73].

The importance for immunomodulatory chemokines in cancer progression is undisputable. The expression of CXCR2 ligands, *CXCL1-3* and *CXCL5-8* by melanoma cells has been shown to control the immune cell composition of the TME, contribute to the ability to escape tumor immune surveillance, induce angiogenesis or define the preferred sites of melanoma metastases [74–77]. In the present study, receptor-ligand analysis revealed that fibroblasts are the major source for cytokines and chemokines (Figure 5D) and not the cancer cells themselves, thus highlighting the importance of fibroblasts in immune cell recruitment and cancer immune surveillance.
Intriguingly, while *CXCL2* was expressed by fibroblasts from all skin cancer types, melanoma-derived CAFs expressed high levels of *CXCL1-3, 5, 6* and *8* and *IL1B* as well as *IL6*, whereas the expression of *CXCL9-11* and *13* was high in non-melanoma CAFs (Figure 5D). *LGALS9*, which has been shown to interact with *CD40* on T cells thereby attenuating their expansion and effector function, was strongly expressed in CAFs from BCC and SCC but not melanoma. Furthermore, HLA genes were highly expressed in CAFs but not normal fibroblasts (Figure 5B), suggesting a role for CAFs as antigen-presenting cells. CAF-mediated cross-presentation of neo-antigens may directly suppress T cell function [78]. These findings indicate that although iCAFs are present in melanoma and non-melanoma skin cancers, the expression of chemokines and possibly other immunomodulating genes is tumor type-dependent. We substantiated the presence of differential crosstalk among tumor types and stages by testing the effect of conditioned medium from various cancer cell lines on healthy-skin derived fibroblasts. Indeed, conditioned medium from metastasis-derived melanoma cell lines induced an iCAF-like phenotype and cytokine/chemokine expression while conditioned medium of a primary melanoma cell line did not change the cytokine/chemokine expression (Figure 6C).

In addition to the fibroblast heterogeneity in skin tumors, our data highlight the tremendous effect of the TME on all cells within a tumor. For example, melanocytes from BCC and SCC samples (tMC), which are part of the non-neoplastic cells in these tumor types, cluster separately from melanocytes that were derived from healthy skin samples (hMC) (Figure 2B and S2C). This indicates that the altered gene expression profile is likely induced by the TME. Further, our CNV analysis clearly shows that samples from the same tumor subtype (Melanoma I – III: Acral lentiginous melanoma, ALM) and body location can greatly differ at molecular level, which explains donor-specific clustering.

In summary, our work provides a cellular and molecular atlas of the three most frequent skin cancer types comprising neoplastic epithelial, mesenchymal, and immune cells. We further reveal and characterize three distinct CAF subsets and show that their abundance and associated signaling molecules and structural proteins critically impact the TME. Therefore, determining the predominant CAF subset within tumor samples may improve future diagnostic strategies and thereby open new avenues for better personalized therapies.

Moreover, pharmacologically targeting CAFs to reduce ECM density could enhance T cell trafficking into tumor nests and thus the efficacy of checkpoint inhibition therapy as well as the penetration of agents that directly target cancer cells.

Methods:

Human healthy skin and tumor samples

Fresh 4 mm punch biopsies from central tumor and unaffected skin adjacent to tumors as well as 10x10 cm healthy skin samples from abdominal plastic surgeries were subjected to cell isolation procedure directly after surgery.

Healthy skin samples III-IV were cut into thin strips after removal of the fat layer. Epidermis was separated from dermis by Dispase 2 (1:100, Roche #04942078001, 20mg/mL), digested in PBS at 37°C for one hour before being peeled off. The epidermal sheet was minced and then subjected to enzymatic digestion in Trypsin-EDTA (GIBCO #25300-054) for 20 min at 37°C in a shaking water bath (Epidermal sheet protocol for enrichment of keratinocytes). Healthy skin dermis and tumor samples were cut into tiny pieces and digested with Collagenase 1 (1:100, GIBCO #17100-017, 50mg/mL), Collagenase 2 (1:100, GIBCO #17101-015, 50mg/mL), Collagenase 4 (1:100, Sigma-Aldrich #C5138, 50mg/mL), Hyaluronidase (1:100, Sigma-Aldrich #H3884, 10mg/mL) and DNAseI (1:250, Sigma-Aldrich #DN25, 5 mg/mL) in DMEM/10%FCS for one hour in a 37°C water bath (Protocol for enrichment of fibroblasts, keratinocytes and immune cells). After enzymatic digestion, the cell suspension was filtered and washed in PBS/10% FCS twice before subjecting it to FACS staining.

After Fc blocking (1:500, CD16/CD32 BD #553142, RRID:AB_394656), cell suspensions were stained for 30 min at 4°C in the dark with CD45-BV605 (1:50, BioLegend #304042, RRID:AB_2562106), ITGA6-PeCy7 (1:100, BioLegend #313622, RRID:AB_2561705), CDH1-PeCy7 (1:200, BioLegend #147310, RRID:AB_2564188), FAP-APC (1:20, R&D Systems #FAB3715A, RRID:AB_2884010), CD90-AF700 (1:30, BioLegend #328120, RRID:AB_2203302) and CD31-FITC (1:30, BD Biosciences #563807), CD106-Pacific Blue (1:100, BD Biosciences #744309, RRID:AB_2742138), CD235ab-Pacific Blue (1:1000, BioLegend #306611, RRID:AB_2248153) and DAPI. ITGA6$^+$/CDH1$^+$ keratinocytes, FAP$^+$/CD90$^+$ fibroblasts, CD45$^+$ immune cells and FAP$^-$CD90$^-$ double negative cells were single cell sorted directly into Smart-seq2 lysis buffer in 384-well plates. After sorting, plates were stored at -80°C until they were sent for sequencing to the Eukaryotic Single Cell Genomics Facility (ESCG) at SciLifeLab at the Karolinska Institutet, Sweden.

Ethical approval

Written informed patient consent was obtained before tissue collection in accordance with the Declaration of Helsinki. Our study was approved by the Institutional Review Board under the ethical permits EK#1695/2021, EK#1783/2020 and EK#1555/2016.

Immunohistochemistry

We performed immunohistochemistry on 4μm human FFPE sections according to standard protocols. Antigen retrieval was conducted in citrate buffer, pH 6.0 and 3%BSA/PBST was used for blocking. Primary antibodies against CD90 (THY1) (1:200, rabbit monoclonal [EPR3133], Abcam #ab133350, RRID:AB_11155503), FAP (1:200, rabbit monoclonal [D3V8A], Cell signaling #13801, RRID:AB_2798316), TAGLN (1:12.000, rabbit polyclonal, Thermo Scientific

#PA5-27463, RRID:AB_2544939), DES (1:2000, rabbit monoclonal [Y266], Abcam #ab32362, RRID:AB_731901), CD31 (1:500, rabbit, Neomarkers, #RB10333-P1)) and COL11A1 (1:200, rabbit polyclonal, Abcam #ab64883, RRID:AB_1140613) were diluted in 1%BSA/PBST and incubated over night. A biotinylated goat anti-rabbit antibody (1:200, Vector BA-1000) was used as second step and incubated for 30 min at room temperature. Novocastra Streptavidin-HRP (Leica Biosystems Newcastle #RE7104) and Dako AEC+ High sensitivity substrate (Dako #K3469) were used for signal enhancement and development. For counter staining, hematoxylin was used.

RNAScope

RNAScope was conducted by using Multiplex Fluorescent Reagent Kit v2 from Advanced Cell Diagnostics, ACD Bio-Techne (#323135), according to the manufacturer's protocol, with probes for *COL1A1* (#401891-C2), *COL11A1* (#400741-C3), *PTGDS* (#431471-C1), *MMP1* (#412641-C1), *RGS5* (#533421-C3) and *PDGFRA* (#604481-C1). For fluorescence staining, the TSA dyes Fluorescein, Cy3 and Cy5 (Akoyabio) and DAPI as nuclear stain were utilized. The Multiplex Fluorescent Reagent Kit v2 and the RNAscope® 4-Plex Ancillary kit were combined for 4-plex stainings against CXCL2 (#425251), CXCL8 (310381-C2), IL24 (404301-C3) and Col1A1 (401891-C4), or against MMP1 (#412641-C1), Col11A1 (#400741-C2), RGS5 (#533421-C3) and COL1A1 (#401891-C4). Opal™ fluorophores (Opal 520, Opal 570, Opal 620 and Opal 690) were utilized in the 4-plex staining's. Images were captured by Vectra Polaris™ and image analysis was conducted with HALO® image analysis platform.

Fibroblast activation by conditioned media of cancer cells and transcriptomic analysis

Normal healthy dermal fibroblasts (NHDF) were isolated as described above and cultured in DMEM containing 10% FBS and 50 µg/ml Gentamycin in a humidified incubator at 37°C and 5% CO_2. Melanoma cell lines (VM15, VM19, VM26, VM08)[63] were cultured in RPMI1640 (GIBCO #11875093) containing 10% FBS (GIBCO #26140079), 2 mM L-glutamine (GIBCO #25030081) and 50 U/ml streptomycin/penicillin (GIBCO #15070063). SCC13[64] cell line (RRID:CVCL_4029) was cultured in DMEM Glutamax containing 10 % FBS, 2 mM L-glutamine (GIBCO #25030081), 50 U/ml streptomycin/penicillin (GIBCO #15070063), 5µg/ml insulin and 10 µg/ml transferrin. When cells reached 70-80% confluency, they were washed with PBS, and DMEM containing 10% FBS. Conditioned medium (CM) was collected 48 hours later, centrifuged with 300 g for 10 minutes and stored at -20°C.

Fibroblast activation assay: NHDF and cancer cells were seeded into 6 well plates for 24 hours. Then, medium of the NHDF was exchanged with CM derived from cancer cells or NHDF as a control. Cells were harvested 72 hours later. RNA was isolated with the Qiagen RNeasy Mini Kit (Qiagen #74106). RevertAid H Minus First Strand cDNA Synthesis Kit (Thermo Scientific #K1631) was used to prepare cDNA after a DNaseI digestion step (Thermo Scientific #EN0521). Taqman 2xUniversal PCR Master Mix (Applied Biosystems #4324018) and Taqman probes for GAPDH (Hs99999905), CXCL1 (Hs00236937_m1), CXCL2 (Hs00601975_m1), CXCL3 (Hs00171061_m1), CXCL5 (Hs01099660_g1), CXCL6 (Hs00605742_g1), CXCL8

(Hs00174103_m1), CCL2 (Hs00234140_m1) and IL24 (Hs01114274_m1) were used in the qPCR analysis. One-way ANOVA followed by Dunnett's multiple comparisons test was performed using GraphPad Prism version 8.0.0 for Windows, GraphPad Software, San Diego, California USA, www.graphpad.com.

Single cell RNA sequencing

scRNA-seq was conducted by the Eukaryotic Single Cell Genomics Facility (ESCG) at SciLifeLab, Sweden according to the Smart-seq2 protocol [79]. Demultiplexed reads were aligned to the human genome (hg19 assembly) and the ERCC spike-in reference using STAR v2.4.2a in two-pass alignment mode [80]. Uniquely aligned reads were transformed into reads per million kilobase (RPKM) using rpkmforgenes . RPKM values were summed up when several isoforms of a gene were detected.

Single cell RNA sequencing data processing

Low quality cells were removed by using thresholds for RPKM-values and number of genes expressed per cell. The lower threshold was referred to empty-well controls, the upper threshold was set based on unusually high RPKM-values of clearly visible outliers. We considered good quality when a minimum of 400 genes and RPKM-values between 150.000-8.000.000 per cell was reached. Finally, 4824 cells were retained after quality control.

Subsequent data analysis was carried out by using R3.6.2 and the Seurat package v3 (Stuart*, Butler*, et al., Cell 2019). RPKM values for each gene per cell were normalized and natural-log transformed (NormalizeData: normalization.method="Log-Normalize"). The 2000 most variable genes were identified (FindVariableGenes: selection.method = 'vst'), the data scaled and principal component analysis (PCA) was performed. The first 20 principal components 1:20, resolution 0.2 and Seurat default parameters were used for UMAP generation of first-level clustering. Subsequently, clusters for second-level clustering were selected based on commonly known signature gene expression: Healthy keratinocytes, SCC and BCC (*KRT5*, *KRT14*), melanocytes and melanoma cells (*MLANA*), immune cells (*CD45*) as well as fibroblasts and vSMCs (*COL1A1*, *RERGL*).

Differentially expressed genes were identified by the Seurat function FindAllMarkers. For generation of UMAPs, violin and bar plots, ggplot2 v3.3.2 were used.

Copy number variations for estimation of malignancy

InferCNV of the Trinity CTAT Project (https://github.com/broadinstitute/inferCNV) was used to calculate CNVs of the tumor samples in comparison to healthy controls. For CreateInfercnvObject, healthy reference controls were grouped into different cell types by ref_group_names=c(Fibroblasts, immune cells, keratinocytes, melanocytes, pericytes/vSMCs, endothelial cells). *InferCNV* operations were performed by infercnv::run using min_cells_per_gene = 3, cutoff = 1, cluster_by_groups = T, denoise = T, HMM = T, analysis_mode = subclusters, hclust_method = ward.D2, tumor_subcluster_partition_method = random_trees. Estimation of malignancy was

performed as previously described [24], using a pearson correlation cutoff of 0.50 and a sum of squares (SoS) cutoff of 0.01.

Heatmaps

ComplexHeatmap v2.2.0 function was used to represent gene expression of single cells or mean gene expression per cluster in heatmaps as z-scores.

Receptor Ligand Analysis

For receptor-ligand pairing the previously published method developed by Simon Joost was used, but with additional adjustments for run-time and parallel computing (Joost et al., 2018)[82]. Receptor-ligand interactions were analyzed between fibroblast clusters, immune cell clusters, neoplastic and healthy keratinocyte and melanocyte clusters.

A signature gene list, containing potential ligands and receptors of each cluster, was generated by the Seurat function FindMarkers() at the level of second-level clustering. Potential ligand-receptor interactions were identified by querying the combined receptor-ligand database from Ramilowski et al., 2015 and Cabello-Aguilar et al., 2020.

For each cluster pair, the number of identified receptor-ligand pairs was compared to the number of pairs obtained from an equally sized randomly sampled pool of receptors and ligands. This was repeated 10.000 times to test for significantly enriched interactions ($p \leq 0.05$ for Benjamini-Hochberg-corrected p-values). An additional prerequisite for a valid receptor-ligand pairing was the presence of at least 2.5% cells of the same donor in both of the potentially interacting clusters (eg. iCAFs interacting with tCD4 requires at least 2.5% cells from the same donor in each of the clusters).

Used packages: *python* 3.7.6, *pandas* 1.0.1, *numpy* 1.18.1, *matplotlib* 3.2.2. Receptor – Ligand heatmaps were generated with *seaborn* 0.11.0 using mean z-scores per donor per cluster.

Module Score

Module Scores were calculated by AddModuleScore() function from Seurat, and genes sets were represented as violin plots. Individual genes of a gene set are shown in heatmaps. Genes that showed absolutely no expression in any cluster were excluded from heatmaps and module score calculation (chemokines: CCL4, CCL14, CXCL7; cytokines: IL9, IL31; MMPs: MMP26). Statistical analysis was done by non-parametric Wilcox rank-sum test using ggplot2 function stat_compare_means().

Melanoma scRNAseq Validation Dataset

For the melanoma validation dataset, pre-treatment samples (n=5) were collected from stage IV melanoma patients as part of a trial investigating anti-CD20 treatment in a therapeutic setting (10.1038/s41467-017-00452-4). After biopsy of a lesion, single cell suspensions were immediately frozen. Thawed suspensions were subjected to scRNA-seq using the Chromium Single Cell Controller and Single Cell 5’ Library & Gel Bead Kit v1.1 (10X Genomics, Pleasanton,

CA) according to the manufacturer's protocol. Sequencing was performed using the Illumina NovaSeq platform and the 150bp paired-end configuration.
Preprocessing of the scRNA-seq data was performed using Cell Ranger version 6.1.2 (10x Genomics). Expression data was processed using R (version 4.2.1) and Seurat (version 4.0.5). Cells with less than 1,000 genes or more than 10% of relative mitochondrial gene counts were removed. The data was processed following Seurat's scTransform workflow. Sample-specific batch effects were corrected using Harmony. Clusters were identified using Seurat's "FindNeighbors" and "FindClusters" functions, using the first 32 dimensions of the Harmony-corrected embedding and a resolution of 1.5. Cell types were subsequently identified based on canonical markers. Heatmaps and module scores were generated as described above.

Publicly available dataset

We reanalyzed the publicly available HNSCC data set (GSE103322) using R3.6.2 and the Seurat package v3 [18]. As described by the authors, we regressed for the variable *processedbyMaximaenzyme*. The cell annotation which was provided in the meta data file was used to select the cells for second-level clustering of the *Fibroblasts*. Based on markers that were described by the authors, the clusters for CAFs, myofibroblasts and intermediate fibroblasts were assigned. A heatmap (ComplexHeatmap v2.2.0) was generated presenting z-scores of mean expression per cluster of the same genes as shown in the heatmap in supplementary figure S2C of the original publication, but extended it by commonly accepted pericyte and vSMC markers. For comparison of gene expression of fibroblasts and cancer cells, the respective cells were selected based on the provided meta data information, and heatmaps as well as module scores were calculated as described above.

Data availability

Raw data are available upon request and count matrices will be uploaded to the EGA repository upon publication.

Funding

This project was supported by funding granted to BML (Austrian Science Fund, FWF, V525-B28; Anniversary Fund of the Austrian National Bank, OeNB, 17855; City of Vienna Fund for innovative interdisciplinary Cancer Research, AP00919OFF; LEO Foundation, LF-AW_EMEA-21-400116), to AF (Hochschuljubiläumsfond of the City of Vienna H-283774/2019), to TJ (Karolinska Institutet, KID), to MK (Swedish Cancer Society, CAN 2018/793; Swedish Research Council, 2018-02963; LEO Foundation, LF-OC-19-000225; Karolinska Institutet, 2-2111/2019), and SNW (Austrian Science Fund, FWF, P31127-B28).

Acknowledgements

We cordially thank Alexander Enz and Matthias Wielscher for assisting with bioinformatic data processing, Robert Loewe and Philipp Weber for their help in sample collection, and Erwin Wagner, Reinhard Kirnbauer and Alessandra Handisurya for their support and critical feedback. Special thanks to Nina Zila, Monika Weiss and Karin Neumüller for their technical assistance and lab organization. We thank Andreas Spittler, Günther Hofbauer as well as Marion Gröger, Sabine Rauscher and Christoph Friedl from the Flow Cytometry and Imaging core facilities of the Medical University Vienna for their continuous support. Finally, we thank the Eukaryotic Single Cell Genomics Facility (ESCG) at SciLifeLab, Sweden for sequencing our cells and the national UPPMAX SENS computational infrastructure for data transfer.

Supplementary Table 1

Donors	Sample type	Body Part	Sex	Age at sampling (yrs)	Histology
BCC I	BCC	capillitium	male	47	Basal cell carcinoma
BCC II	BCC	nose	male	80	Basal cell carcinoma
BCC III	BCC	shoulder	male	77	Basal cell carcinoma
Mel I	Melanoma	heal	male	78	Acral lentiginous melanoma, T4b, thickness 12 mm
Mel II	Melanoma	toe	male	86	Acral lentiginous melanoma, T4b, thickness 8 mm
Mel III	Melanoma	toe	female	87	Acral lentiginous melanoma, T4b, thickness 5 mm
SCC I	SCC	capillitium	male	56	Reoccurrence of poorly differentiated SCC in scar, thickness 3 mm
SCC II	SCC	lower leg	male	78	Highly differentiated SCC, thickness 2 mm
SCC III	SCC	capillitium	male	93	Poorly differentiated SCC, thickness 4 mm
SCC IV	SCC	lower leg	male	92	Bowen carcinoma, thickness 8 mm
Healthy I	Healthy skin	upper arm	female	63	
Healthy II	Healthy skin	abdomen	female	43	
Healthy III	Healthy skin	abdomen	female	59	
Healthy IV	Healthy skin	upper arm	female	44	
Healthy V	Healthy skin	abdomen	male	48	

References:

1. Gieniec, K.A., Butler, L.M., Worthley, D.L., and Woods, S.L. (2019). Cancer-associated fibroblasts—heroes or villains? Br J Cancer *121*, 293–302. 10.1038/s41416-019-0509-3.

2. Kalluri, R. (2016). The biology and function of fibroblasts in cancer. Nat Rev Cancer *16*, 582–598. 10.1038/nrc.2016.73.

3. Li, T., Yang, Y., Hua, X., Wang, G., Liu, W., Jia, C., Tai, Y., Zhang, Q., and Chen, G. (2012). Hepatocellular carcinoma-associated fibroblasts trigger NK cell dysfunction via PGE2 and IDO. Cancer Letters *318*, 154–161. 10.1016/j.canlet.2011.12.020.

4. Mariathasan, S., Turley, S.J., Nickles, D., Castiglioni, A., Yuen, K., Wang, Y., Kadel III, E.E., Koeppen, H., Astarita, J.L., Cubas, R., et al. (2018). TGFβ attenuates tumour response to PD-L1 blockade by contributing to exclusion of T cells. Nature *554*, 544–548. 10.1038/nature25501.

5. Özdemir, B.C., Pentcheva-Hoang, T., Carstens, J.L., Zheng, X., Wu, C.-C., Simpson, T.R., Laklai, H., Sugimoto, H., Kahlert, C., Novitskiy, S.V., et al. (2014). Depletion of Carcinoma-Associated Fibroblasts and Fibrosis Induces Immunosuppression and Accelerates Pancreas Cancer with Reduced Survival. Cancer Cell *25*, 719–734. 10.1016/j.ccr.2014.04.005.

6. Paulsson, J., and Micke, P. (2014). Prognostic relevance of cancer-associated fibroblasts in human cancer. Seminars in Cancer Biology *25*, 61–68. 10.1016/j.semcancer.2014.02.006.

7. Rhim, A.D., Oberstein, P.E., Thomas, D.H., Mirek, E.T., Palermo, C.F., Sastra, S.A., Dekleva, E.N., Saunders, T., Becerra, C.P., Tattersall, I.W., et al. (2014). Stromal Elements Act to Restrain, Rather Than Support, Pancreatic Ductal Adenocarcinoma. Cancer Cell *25*, 735–747. 10.1016/j.ccr.2014.04.021.

8. Lichtenberger, B.M., and Kasper, M. (2021). Cellular heterogeneity and microenvironmental control of skin cancer. J Intern Med *289*, 614–628. 10.1111/joim.13177.

9. Mezawa, Y., and Orimo, A. (2021). Phenotypic heterogeneity, stability and plasticity in tumor-promoting carcinoma-associated fibroblasts. FEBS J, febs.15851. 10.1111/febs.15851.

10. Philippeos, C., Telerman, S.B., Oulès, B., Pisco, A.O., Shaw, T.J., Elgueta, R., Lombardi, G., Driskell, R.R., Soldin, M., Lynch, M.D., et al. (2018). Spatial and Single-Cell Transcriptional Profiling Identifies Functionally Distinct Human Dermal Fibroblast Subpopulations. Journal of Investigative Dermatology *138*, 811–825. 10.1016/j.jid.2018.01.016.

11. Tabib, T., Morse, C., Wang, T., Chen, W., and Lafyatis, R. (2018). SFRP2/DPP4 and FMO1/LSP1 Define Major Fibroblast Populations in Human Skin. Journal of Investigative Dermatology *138*, 802–810. 10.1016/j.jid.2017.09.045.

12. Vorstandlechner, V., Laggner, M., Kalinina, P., Haslik, W., Radtke, C., Shaw, L., Lichtenberger, B.M., Tschachler, E., Ankersmit, H.J., and Mildner, M. (2020). Deciphering the functional heterogeneity of skin fibroblasts using single-cell RNA sequencing. FASEB j. *34*, 3677–3692. 10.1096/fj.201902001RR.

13. Kieffer, Y., Hocine, H.R., Gentric, G., Pelon, F., Bernard, C., Bourachot, B., Lameiras, S., Albergante, L., Bonneau, C., Guyard, A., et al. (2020). Single-Cell Analysis Reveals Fibroblast Clusters Linked to Immunotherapy Resistance in Cancer. Cancer Discov *10*, 1330–1351. 10.1158/2159-8290.CD-19-1384.

14. Norton, J., Foster, D., Chinta, M., Titan, A., and Longaker, M. (2020). Pancreatic Cancer Associated Fibroblasts (CAF): Under-Explored Target for Pancreatic Cancer Treatment. Cancers *12*, 1347. 10.3390/cancers12051347.

15. Wang, Y., Liang, Y., Xu, H., Zhang, X., Mao, T., Cui, J., Yao, J., Wang, Y., Jiao, F., Xiao, X., et al. (2021). Single-cell analysis of pancreatic ductal adenocarcinoma identifies a novel fibroblast subtype associated with poor prognosis but better immunotherapy response. Cell Discov *7*, 36. 10.1038/s41421-021-00271-4.

16. Khaliq, A.M., Kurt, Z., Grunvald, M.W., Erdogan, C., Turgut, S.S., Rand, T., Khare, S., Borgia, J.A., Hayden, D.M., Pappas, S.G., et al. (2021). Redefining tumor classification and clinical stratification through a colorectal cancer single-cell atlas. bioRxiv, 2021.02.02.429256. 10.1101/2021.02.02.429256.

17. Pelka, K., Hofree, M., Chen, J.H., Sarkizova, S., Pirl, J.D., Jorgji, V., Bejnood, A., Dionne, D., Ge, W.H., Xu, K.H., et al. (2021). Spatially organized multicellular immune hubs in human colorectal cancer. Cell *184*, 4734-4752.e20. 10.1016/j.cell.2021.08.003.

18. Puram, S.V., Tirosh, I., Parikh, A.S., Patel, A.P., Yizhak, K., Gillespie, S., Rodman, C., Luo, C.L., Mroz, E.A., Emerick, K.S., et al. (2017). Single-Cell Transcriptomic Analysis of Primary and Metastatic Tumor Ecosystems in Head and Neck Cancer. Cell *171*, 1611-1624.e24. 10.1016/j.cell.2017.10.044.

19. Guo, T., Li, W., and Cai, X. (2020). Applications of Single-Cell Omics to Dissect Tumor Microenvironment. Front. Genet. *11*, 548719. 10.3389/fgene.2020.548719.

20. Jerby-Arnon, L., Shah, P., Cuoco, M.S., Rodman, C., Su, M.-J., Melms, J.C., Leeson, R., Kanodia, A., Mei, S., Lin, J.-R., et al. (2018). A Cancer Cell Program Promotes T Cell Exclusion and Resistance to Checkpoint Blockade. Cell *175*, 984-997.e24. 10.1016/j.cell.2018.09.006.

21. Ji, A.L., Rubin, A.J., Thrane, K., Jiang, S., Reynolds, D.L., Meyers, R.M., Guo, M.G., George, B.M., Mollbrink, A., Bergenstråhle, J., et al. (2020). Multimodal Analysis of Composition and Spatial Architecture in Human Squamous Cell Carcinoma. Cell *182*, 497-514.e22. 10.1016/j.cell.2020.05.039.

22. Li, H., van der Leun, A.M., Yofe, I., Lubling, Y., Gelbard-Solodkin, D., van Akkooi, A.C.J., van den Braber, M., Rozeman, E.A., Haanen, J.B.A.G., Blank, C.U., et al. (2019). Dysfunctional CD8 T Cells Form a Proliferative, Dynamically Regulated Compartment within Human Melanoma. Cell *176*, 775-789.e18. 10.1016/j.cell.2018.11.043.

23. Sade-Feldman, M., Yizhak, K., Bjorgaard, S.L., Ray, J.P., de Boer, C.G., Jenkins, R.W., Lieb, D.J., Chen, J.H., Frederick, D.T., Barzily-Rokni, M., et al. (2018). Defining T Cell States Associated with Response to Checkpoint Immunotherapy in Melanoma. Cell *175*, 998-1013.e20. 10.1016/j.cell.2018.10.038.

24. Tirosh, I., Izar, B., Prakadan, S.M., Wadsworth, M.H., Treacy, D., Trombetta, J.J., Rotem, A., Rodman, C., Lian, C., Murphy, G., et al. (2016). Dissecting the multicellular ecosystem of metastatic melanoma by single-cell RNA-seq. Science *352*, 189–196. 10.1126/science.aad0501.

25. Yost, K.E., Satpathy, A.T., Wells, D.K., Qi, Y., Wang, C., Kageyama, R., McNamara, K.L., Granja, J.M., Sarin, K.Y., Brown, R.A., et al. (2019). Clonal replacement of tumor-specific T cells following PD-1 blockade. Nat Med *25*, 1251–1259. 10.1038/s41591-019-0522-3.

26. Gao, Y., Li, X., Zeng, C., Liu, C., Hao, Q., Li, W., Zhang, K., Zhang, W., Wang, S., Zhao, H., et al. (2020). CD63 $^{+}$ Cancer-Associated Fibroblasts Confer Tamoxifen Resistance to Breast Cancer Cells through Exosomal miR-22. Adv. Sci. *7*, 2002518. 10.1002/advs.202002518.

27. Ishibashi, M., Neri, S., Hashimoto, H., Miyashita, T., Yoshida, T., Nakamura, Y., Udagawa, H., Kirita, K., Matsumoto, S., Umemura, S., et al. (2017). CD200-positive cancer associated fibroblasts augment the sensitivity of Epidermal Growth Factor Receptor mutation-positive lung adenocarcinomas to EGFR Tyrosine kinase inhibitors. Sci Rep *7*, 46662. 10.1038/srep46662.

28. Su, S., Chen, J., Yao, H., Liu, J., Yu, S., Lao, L., Wang, M., Luo, M., Xing, Y., Chen, F., et al. (2018). CD10+GPR77+ Cancer-Associated Fibroblasts Promote Cancer Formation and Chemoresistance by Sustaining Cancer Stemness. Cell *172*, 841-856.e16. 10.1016/j.cell.2018.01.009.

29. Chen, Z., Zhou, L., Liu, L., Hou, Y., Xiong, M., Yang, Y., Hu, J., and Chen, K. (2020). Single-cell RNA sequencing highlights the role of inflammatory cancer-associated fibroblasts in bladder urothelial carcinoma. Nat Commun *11*, 5077. 10.1038/s41467-020-18916-5.

30. Elyada, E., Bolisetty, M., Laise, P., Flynn, W.F., Courtois, E.T., Burkhart, R.A., Teinor, J.A., Belleau, P., Biffi, G., Lucito, M.S., et al. (2019). Cross-Species Single-Cell Analysis of Pancreatic Ductal Adenocarcinoma Reveals Antigen-Presenting Cancer-Associated Fibroblasts. Cancer Discov *9*, 1102–1123. 10.1158/2159-8290.CD-19-0094.

31. Geng, X., Chen, H., Zhao, L., Hu, J., Yang, W., Li, G., Cheng, C., Zhao, Z., Zhang, T., Li, L., et al. (2021). Cancer-Associated Fibroblast (CAF) Heterogeneity and Targeting Therapy of CAFs in Pancreatic Cancer. Front. Cell Dev. Biol. *9*, 655152. 10.3389/fcell.2021.655152.

32. Öhlund, D., Handly-Santana, A., Biffi, G., Elyada, E., Almeida, A.S., Ponz-Sarvise, M., Corbo, V., Oni, T.E., Hearn, S.A., Lee, E.J., et al. (2017). Distinct populations of inflammatory fibroblasts and myofibroblasts in pancreatic cancer. Journal of Experimental Medicine *214*, 579–596. 10.1084/jem.20162024.

33. Sahai, E., Astsaturov, I., Cukierman, E., DeNardo, D.G., Egeblad, M., Evans, R.M., Fearon, D., Greten, F.R., Hingorani, S.R., Hunter, T., et al. (2020). A framework for advancing our understanding of cancer-associated fibroblasts. Nat Rev Cancer *20*, 174–186. 10.1038/s41568-019-0238-1.

34. Van Hove, L., and Hoste, E. (2021). Activation of Fibroblasts in Skin Cancer. Journal of Investigative Dermatology, S0022202X21022892. 10.1016/j.jid.2021.09.010.

35. Driskell, R.R., Lichtenberger, B.M., Hoste, E., Kretzschmar, K., Simons, B.D., Charalambous, M., Ferron, S.R., Herault, Y., Pavlovic, G., Ferguson-Smith, A.C., et al. (2013). Distinct fibroblast lineages determine dermal architecture in skin development and repair. Nature *504*, 277–281. 10.1038/nature12783.

36. Jiang, D., Correa-Gallegos, D., Christ, S., Stefanska, A., Liu, J., Ramesh, P., Rajendran, V., De Santis, M.M., Wagner, D.E., and Rinkevich, Y. (2018). Two succeeding fibroblastic lineages drive dermal development and the transition from regeneration to scarring. Nat Cell Biol *20*, 422–431. 10.1038/s41556-018-0073-8.

37. Korosec, A., Frech, S., Gesslbauer, B., Vierhapper, M., Radtke, C., Petzelbauer, P., and Lichtenberger, B.M. (2019). Lineage Identity and Location within the Dermis Determine the Function of Papillary and Reticular Fibroblasts in Human Skin. Journal of Investigative Dermatology *139*, 342–351. 10.1016/j.jid.2018.07.033.

38. Rinkevich, Y., Walmsley, G.G., Hu, M.S., Maan, Z.N., Newman, A.M., Drukker, M., Januszyk, M., Krampitz, G.W., Gurtner, G.C., Lorenz, H.P., et al. (2015). Identification and isolation of a dermal lineage with intrinsic fibrogenic potential. Science *348*, aaa2151. 10.1126/science.aaa2151.

39. Omland, S.H., Wettergren, E.E., Mollerup, S., Asplund, M., Mourier, T., Hansen, A.J., and Gniadecki, R. (2017). Cancer associated fibroblasts (CAFs) are activated in cutaneous basal cell carcinoma and in the peritumoural skin. BMC Cancer *17*, 675. 10.1186/s12885-017-3663-0.

40. Papaccio, F., Kovacs, D., Bellei, B., Caputo, S., Migliano, E., Cota, C., and Picardo, M. (2021). Profiling Cancer-Associated Fibroblasts in Melanoma. IJMS *22*, 7255. 10.3390/ijms22147255.

41. Sasaki, K., Sugai, T., Ishida, K., Osakabe, M., Amano, H., Kimura, H., Sakuraba, M., Kashiwa, K., and Kobayashi, S. (2018). Analysis of cancer-associated fibroblasts and the epithelial-mesenchymal transition in cutaneous basal cell carcinoma, squamous cell carcinoma, and malignant melanoma. Human Pathology *79*, 1–8. 10.1016/j.humpath.2018.03.006.

42. Waldman, A., and Schmults, C. (2019). Cutaneous Squamous Cell Carcinoma. Hematology/Oncology Clinics of North America *33*, 1–12. 10.1016/j.hoc.2018.08.001.

43. Kim, D.P., Kus, K.J.B., and Ruiz, E. (2019). Basal Cell Carcinoma Review. Hematology/Oncology Clinics of North America *33*, 13–24. 10.1016/j.hoc.2018.09.004.

44. Miller, A.J., and Mihm, M.C. (2006). Melanoma. N Engl J Med *355*, 51–65. 10.1056/NEJMra052166.

45. Kurokawa, I., Takahashi, K., Moll, I., and Moll, R. (2011). Expression of keratins in cutaneous epithelial tumors and related disorders - distribution and clinical significance: Keratin expression in cutaneous epithelial tumors. Experimental Dermatology *20*, 217–228. 10.1111/j.1600-0625.2009.01006.x.

46. Hutchin, M.E., Kariapper, M.S.T., Grachtchouk, M., Wang, A., Wei, L., Cummings, D., Liu, J., Michael, L.E., Glick, A., and Dlugosz, A.A. (2005). Sustained Hedgehog signaling is required for basal cell carcinoma proliferation and survival: conditional skin tumorigenesis recapitulates the hair growth cycle. Genes Dev. *19*, 214–223. 10.1101/gad.1258705.

47. Reynolds, G., Vegh, P., Fletcher, J., Poyner, E.F.M., Stephenson, E., Goh, I., Botting, R.A., Huang, N., Olabi, B., Dubois, A., et al. (2021). Developmental cell programs are co-opted in inflammatory skin disease. Science *371*, eaba6500. 10.1126/science.aba6500.

48. Alexandrov, L.B., Nik-Zainal, S., Wedge, D.C., Aparicio, S.A.J.R., Behjati, S., Biankin, A.V., Bignell, G.R., Bolli, N., Borg, A., Børresen-Dale, A.-L., et al. (2013). Signatures of mutational processes in human cancer. Nature *500*, 415–421. 10.1038/nature12477.

49. Dotto, G.P. (2014). Multifocal epithelial tumors and field cancerization: stroma as a primary determinant. J. Clin. Invest. *124*, 1446–1453. 10.1172/JCI72589.

50. Shimomura, Y., Agalliu, D., Vonica, A., Luria, V., Wajid, M., Baumer, A., Belli, S., Petukhova, L., Schinzel, A., Brivanlou, A.H., et al. (2010). APCDD1 is a novel Wnt inhibitor mutated in hereditary hypotrichosis simplex. Nature *464*, 1043–1047. 10.1038/nature08875.

51. Janson, D.G., Saintigny, G., van Adrichem, A., Mahé, C., and El Ghalbzouri, A. (2012). Different Gene Expression Patterns in Human Papillary and Reticular Fibroblasts. Journal of Investigative Dermatology *132*, 2565–2572. 10.1038/jid.2012.192.

52. Hinz, B. (2016). The role of myofibroblasts in wound healing. Current Research in Translational Medicine *64*, 171–177. 10.1016/j.retram.2016.09.003.

53. Armulik, A., Genové, G., and Betsholtz, C. (2011). Pericytes: Developmental, Physiological, and Pathological Perspectives, Problems, and Promises. Developmental Cell *21*, 193–215. 10.1016/j.devcel.2011.07.001.

54. He, H., Suryawanshi, H., Morozov, P., Gay-Mimbrera, J., Del Duca, E., Kim, H.J., Kameyama, N., Estrada, Y., Der, E., Krueger, J.G., et al. (2020). Single-cell transcriptome analysis of human skin identifies novel fibroblast subpopulation and enrichment of immune subsets in atopic dermatitis. Journal of Allergy and Clinical Immunology *145*, 1615–1628. 10.1016/j.jaci.2020.01.042.

55. Paquet-Fifield, S., Schlüter, H., Li, A., Aitken, T., Gangatirkar, P., Blashki, D., Koelmeyer, R., Pouliot, N., Palatsides, M., Ellis, S., et al. (2009). A role for pericytes as

microenvironmental regulators of human skin tissue regeneration. J. Clin. Invest., JCI38535. 10.1172/JCI38535.

56. Crisan, M., Yap, S., Casteilla, L., Chen, C.-W., Corselli, M., Park, T.S., Andriolo, G., Sun, B., Zheng, B., Zhang, L., et al. (2008). A Perivascular Origin for Mesenchymal Stem Cells in Multiple Human Organs. Cell Stem Cell *3*, 301–313. 10.1016/j.stem.2008.07.003.

57. Nurmik, M., Ullmann, P., Rodriguez, F., Haan, S., and Letellier, E. (2020). In search of definitions: Cancer-associated fibroblasts and their markers. Int. J. Cancer *146*, 895–905. 10.1002/ijc.32193.

58. Bartoschek, M., Oskolkov, N., Bocci, M., Lövrot, J., Larsson, C., Sommarin, M., Madsen, C.D., Lindgren, D., Pekar, G., Karlsson, G., et al. (2018). Spatially and functionally distinct subclasses of breast cancer-associated fibroblasts revealed by single cell RNA sequencing. Nat Commun *9*, 5150. 10.1038/s41467-018-07582-3.

59. Hughes, S., and Chan-Ling, T. (2004). Characterization of Smooth Muscle Cell and Pericyte Differentiation in the Rat Retina In Vivo. Invest. Ophthalmol. Vis. Sci. *45*, 2795. 10.1167/iovs.03-1312.

60. Stapor, P.C., Sweat, R.S., Dashti, D.C., Betancourt, A.M., and Murfee, W.L. (2014). Pericyte Dynamics during Angiogenesis: New Insights from New Identities. J Vasc Res *51*, 163–174. 10.1159/000362276.

61. Dominguez, C.X., Müller, S., Keerthivasan, S., Koeppen, H., Hung, J., Gierke, S., Breart, B., Foreman, O., Bainbridge, T.W., Castiglioni, A., et al. (2020). Single-Cell RNA Sequencing Reveals Stromal Evolution into LRRC15 $^{+}$ Myofibroblasts as a Determinant of Patient Response to Cancer Immunotherapy. Cancer Discov *10*, 232–253. 10.1158/2159-8290.CD-19-0644.

62. Grout, J.A., Sirven, P., Leader, A.M., Maskey, S., Hector, E., Puisieux, I., Steffan, F., Cheng, E., Tung, N., Maurin, M., et al. (2022). Spatial Positioning and Matrix Programs of Cancer-Associated Fibroblasts Promote T-cell Exclusion in Human Lung Tumors. Cancer Discovery *12*, 2606–2625. 10.1158/2159-8290.CD-21-1714.

63. Berger, W., Hauptmann, E., Elbling, L., Vetterlein, M., Kokoschka, E.M., and Micksche, M. (1997). Possible role of the multidrug resistance-associated protein (MRP) in chemoresistance of human melanoma cells. Int. J. Cancer *71*, 108–115. 10.1002/(SICI)1097-0215(19970328)71:1<108::AID-IJC18>3.0.CO;2-E.

64. Lefort, K., Mandinova, A., Ostano, P., Kolev, V., Calpini, V., Kolfschoten, I., Devgan, V., Lieb, J., Raffoul, W., Hohl, D., et al. (2007). Notch1 is a p53 target gene involved in human keratinocyte tumor suppression through negative regulation of ROCK1/2 and MRCKα kinases. Genes Dev. *21*, 562–577. 10.1101/gad.1484707.

65. Ping, Q., Yan, R., Cheng, X., Wang, W., Zhong, Y., Hou, Z., Shi, Y., Wang, C., and Li, R. (2021). Cancer-associated fibroblasts: overview, progress, challenges, and directions. Cancer Gene Ther *28*, 984–999. 10.1038/s41417-021-00318-4.

66. Hosaka, K., Yang, Y., Seki, T., Fischer, C., Dubey, O., Fredlund, E., Hartman, J., Religa, P., Morikawa, H., Ishii, Y., et al. (2016). Pericyte–fibroblast transition promotes tumor growth and metastasis. Proc Natl Acad Sci USA *113*, E5618–E5627. 10.1073/pnas.1608384113.

67. Luo, H., Xia, X., Huang, L.-B., An, H., Cao, M., Kim, G.D., Chen, H.-N., Zhang, W.-H., Shu, Y., Kong, X., et al. (2022). Pan-cancer single-cell analysis reveals the heterogeneity and plasticity of cancer-associated fibroblasts in the tumor microenvironment. Nat Commun *13*, 6619. 10.1038/s41467-022-34395-2.

68. Foster, D.S., Jones, R.E., Ransom, R.C., Longaker, M.T., and Norton, J.A. (2018). The evolving relationship of wound healing and tumor stroma. JCI Insight *3*, e99911. 10.1172/jci.insight.99911.

69. Otranto, M., Sarrazy, V., Bonté, F., Hinz, B., Gabbiani, G., and Desmouliere, A. (2012). The role of the myofibroblast in tumor stroma remodeling. Cell Adhesion & Migration *6*, 203–219. 10.4161/cam.20377.

70. Brown, F.D., and Turley, S.J. (2015). Fibroblastic Reticular Cells: Organization and Regulation of the T Lymphocyte Life Cycle. The Journal of Immunology *194*, 1389–1394. 10.4049/jimmunol.1402520.

71. Koppensteiner, L., Mathieson, L., O'Connor, R.A., and Akram, A.R. (2022). Cancer Associated Fibroblasts - An Impediment to Effective Anti-Cancer T Cell Immunity. Front. Immunol. *13*, 887380. 10.3389/fimmu.2022.887380.

72. Ford, K., Hanley, C.J., Mellone, M., Szyndralewiez, C., Heitz, F., Wiesel, P., Wood, O., Machado, M., Lopez, M.-A., Ganesan, A.-P., et al. (2020). NOX4 Inhibition Potentiates Immunotherapy by Overcoming Cancer-Associated Fibroblast-Mediated CD8 T-cell Exclusion from Tumors. Cancer Research *80*, 1846–1860. 10.1158/0008-5472.CAN-19-3158.

73. Ziani, L., Chouaib, S., and Thiery, J. (2018). Alteration of the Antitumor Immune Response by Cancer-Associated Fibroblasts. Front. Immunol. *9*, 414. 10.3389/fimmu.2018.00414.

74. Dhawan, P., and Richmond, A. (2017). Role of CXCL1 in tumorigenesis of melanoma. 11.

75. Forsthuber, A., Lipp, K., Andersen, L., Ebersberger, S., Graña-Castro, 'Osvaldo, Ellmeier, W., Petzelbauer, P., Lichtenberger, B.M., and Loewe, R. (2019). CXCL5 as Regulator of Neutrophil Function in Cutaneous Melanoma. Journal of Investigative Dermatology *139*, 186–194. 10.1016/j.jid.2018.07.006.

76. Payne, A.S., and Cornelius, L.A. (2002). The Role of Chemokines in Melanoma Tumor Growth and Metastasis. Journal of Investigative Dermatology *118*, 915–922. 10.1046/j.1523-1747.2002.01725.x.

77. Soler-Cardona, A., Forsthuber, A., Lipp, K., Ebersberger, S., Heinz, M., Schossleitner, K., Buchberger, E., Gröger, M., Petzelbauer, P., Hoeller, C., et al. (2018). CXCL5 Facilitates

Melanoma Cell–Neutrophil Interaction and Lymph Node Metastasis. Journal of Investigative Dermatology *138*, 1627–1635. 10.1016/j.jid.2018.01.035.

78. Harryvan, T.J., Visser, M., de Bruin, L., Plug, L., Griffioen, L., Mulder, A., van Veelen, P.A., van der Heden van Noort, G.J., Jongsma, M.L., Meeuwsen, M.H., et al. (2022). Enhanced antigen cross-presentation in human colorectal cancer-associated fibroblasts through upregulation of the lysosomal protease cathepsin S. J Immunother Cancer *10*, e003591. 10.1136/jitc-2021-003591.

79. Picelli, S., Björklund, Å.K., Faridani, O.R., Sagasser, S., Winberg, G., and Sandberg, R. (2013). Smart-seq2 for sensitive full-length transcriptome profiling in single cells. Nat Methods *10*, 1096–1098. 10.1038/nmeth.2639.

80. Dobin, A., and Gingeras, T.R. (2015). Mapping RNA-seq Reads with STAR. Curr Protoc Bioinformatics *51*, 11.14.1-11.14.19. 10.1002/0471250953.bi1114s51.

81. Ramsköld, D., Luo, S., Wang, Y.-C., Li, R., Deng, Q., Faridani, O.R., Daniels, G.A., Khrebtukova, I., Loring, J.F., Laurent, L.C., et al. (2012). Full-length mRNA-Seq from single-cell levels of RNA and individual circulating tumor cells. Nature Biotechnology *30*, 777–782. 10.1038/nbt.2282.

82. Joost, S., Jacob, T., Sun, X., Annusver, K., La Manno, G., Sur, I., and Kasper, M. (2018). Single-Cell Transcriptomics of Traced Epidermal and Hair Follicle Stem Cells Reveals Rapid Adaptations during Wound Healing. Cell Reports *25*, 585-597.e7. 10.1016/j.celrep.2018.09.059.

83. Ramilowski, J.A., Goldberg, T., Harshbarger, J., Kloppmann, E., Lizio, M., Satagopam, V.P., Itoh, M., Kawaji, H., Carninci, P., Rost, B., et al. (2015). A draft network of ligand–receptor-mediated multicellular signalling in human. Nat Commun *6*, 7866. 10.1038/ncomms8866.

84. Cabello-Aguilar, S., Alame, M., Kon-Sun-Tack, F., Fau, C., Lacroix, M., and Colinge, J. (2020). SingleCellSignalR: inference of intercellular networks from single-cell transcriptomics. Nucleic Acids Research *48*, e55–e55. 10.1093/nar/gkaa183.

Figure Legends:

Figure 1. A single cell transcriptomic atlas of human BCC, SCC, melanoma and healthy skin.

(A) Workflow of donor sample processing for Smart-seq2 scRNA-seq, data analysis and verification.

(B) UMAP projection of first-level clustering of 4824 cells (left). Clusters are labelled by cell types, which were identified by commonly accepted marker genes (right).

(C) Expression of top marker genes for the main cell types.

Figure 2. Second-level clustering of non-mesenchymal cells and CNV analysis.

(A-B) UMAP projection of second-level clustering, violin plots of signature genes as well as bar plots showing donor sample distribution per cluster are presented for healthy and neoplastic keratinocytes and melanocytes.

(C) CNV analysis (based on *inferCNV* package) of tumor samples using healthy skin as reference controls. UMAPs for healthy and neoplastic keratinocytes and melanocytes: Malignant cells with a predicted CNV alteration are highlighted in red and *PTCH1* and *PTCH2* overexpressing cells without CNVs are highlighted in orange.

(D) UMAP projection of second-level clustering, violin plots of signature genes as well as bar plots showing donor sample distribution per cluster are presented for immune cells. The distribution of cytotoxic, helper and regulatory T cells are depicted in separate cut-outs.

(E) Heatmap of genes that reflect the resting, activation, cytotoxic, co-stimulatory or co-inhibitors status of T cell subsets from healthy and tumor samples. KC-keratinocyte, MC-melanocyte, MEL-melanoma cells, hTcells-healthy T cells, tCD8-Cytotoxic T cells, tCD4-Helper T cells, Tregs-Regulatory T cells.

Figure 3. Second-level clustering of fibroblasts and vascular smooth muscle cells (vSMCs) results in two heathy fibroblasts populations, fours CAF subsets and one vSMC cluster.

(A) UMAP of second-level clustered fibroblasts and vSMCs. Violin plots of signature genes and bar plots showing donor sample distribution per cluster.

(B) Heatmap of top ten differentially expressed genes per cluster.

Figure 4. The RGS5$^+$ cells are an inhomogeneous population of CAFs and pericytes.

(A) Feature and violin plots showing the expression of fibroblast and pericyte marker genes in the RGS5$^+$ cluster. Representative immunohistochemistry of TAGLN, DES and CD31 in different regions of the tumor (intratumoral, peritumoral).

(B) Representative images of *COL1A1* (green), *RGS5* (red) and *PDGFRA* (blue) RNAScope fluorescence stainings in four different regions of FFPE tissue sections from donor sample SCC IV. DAPI nuclear stain is shown in grey. Scale bar represents 20 μm.

(C) Myofibroblasts in a HNSCC dataset from Puram et al. 2017, exhibits a very similar expression pattern in comparison to the RGS5$^+$ cluster in our dataset.

Figure 5. mCAFs and iCAFs are characterized by the expression of ECM and immunomodulatory genes, respectively.

Representative images from (A) *COL1A1* (green), *COL11A1* (red) and *PTGDS* (blue) and (B) *COL1A1* (green) and *MMP1* (red) RNAScope fluorescence stainings to identifiy mCAFs and iCAFs respectively in FFPE tissue sections from different tumor samples. DAPI nuclear stain is shown in grey. Scale bar represents 20 μm.

Expression of (C) matrix-associated genes in mCAFs and (D) immunomodulatory genes in iCAFs compared to healthy and neoplastic keratinocytes and melanocytes. Interrogation for receptors in healthy and neoplastic keratinocytes and melanocytes as well as immune cells.

Figure 6. Fibroblasts are an important source of chemokines in the tumor.

(A) Representative images of RNA ISH staining with probes against *CXCL2*, *CXCL8*, *IL24* and *COL1A1* of SCC and nodular melanoma samples.

(B) In 29 tissue sections (4 BCCs (non-infiltrative), 4 infiltrative BCCs, 4 differentiated SCCs, 4 undifferentiated SCCs, 6 superficially spreading melanomas and 7 nodular melanomas) the content of cytokine expressing CAFs was evaluated. Each sample was grouped into one of the 3 categories: No iCAFs, single iCAFs and many iCAFs.

(C) *In vitro* cytokine expression of NHDF after exposure to conditioned media from NHDF, VM08, VM15, VM19 and SCC13 cells for 72 hours in comparison to the cytokine expression of the cancer cell lines VM08, VM15, VM19 and SCC13.

(D) Schematic summary of spatial distribution of distinct CAF subsets in human skin cancer.

Figure 1

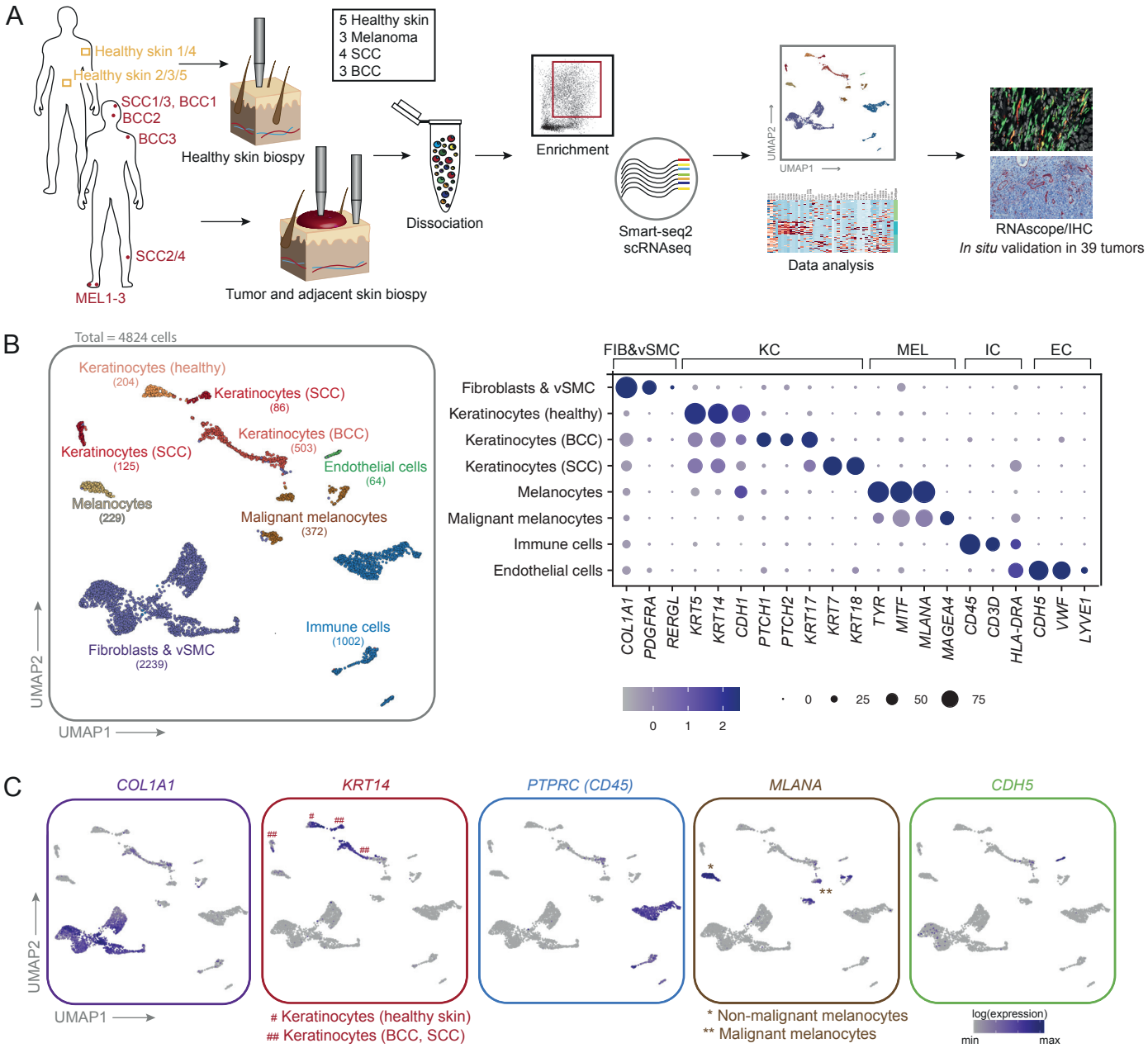
A
Healthy skin 1/4
Healthy skin 2/3/5
SCC1/3, BCC1
BCC2
BCC3
SCC2/4
MEL1-3
Healthy skin biopsy
Tumor and adjacent skin biopsy
5 Healthy skin
3 Melanoma
4 SCC
3 BCC
Dissociation
Enrichment
Smart-seq2
scRNAseq
UMAP2
UMAP1
Data analysis
RNAscope/IHC
In situ validation in 39 tumors
B
Total = 4824 cells
Keratinocytes (healthy)
(204)
Keratinocytes (SCC)
(86)
Keratinocytes (BCC)
(503)
Keratinocytes (SCC)
(125)
Endothelial cells
(64)
Melanocytes
(229)
Malignant melanocytes
(372)
Immune cells
(1002)
Fibroblasts & vSMC
(2239)
UMAP2
UMAP1
FIB&vSMC
KC
MEL
IC
EC
Fibroblasts & vSMC
Keratinocytes (healthy)
Keratinocytes (BCC)
Keratinocytes (SCC)
Melanocytes
Malignant melanocytes
Immune cells
Endothelial cells
COL1A1
PDGFRA
RERGL
KRT5
KRT14
CDH1
PTCH1
PTCH2
KRT17
KRT7
KRT18
TYR
MITF
MLANA
MAGEA4
CD45
CD3D
HLA-DRA
CDH5
VWF
LYVE1
0
1
2
0
25
50
75
C
COL1A1
KRT14
PTPRC (CD45)
MLANA
CDH5
UMAP2
UMAP1
Keratinocytes (healthy skin)
Keratinocytes (BCC, SCC)
* Non-malignant melanocytes
** Malignant melanocytes
log(expression)
min
max

Figure 2

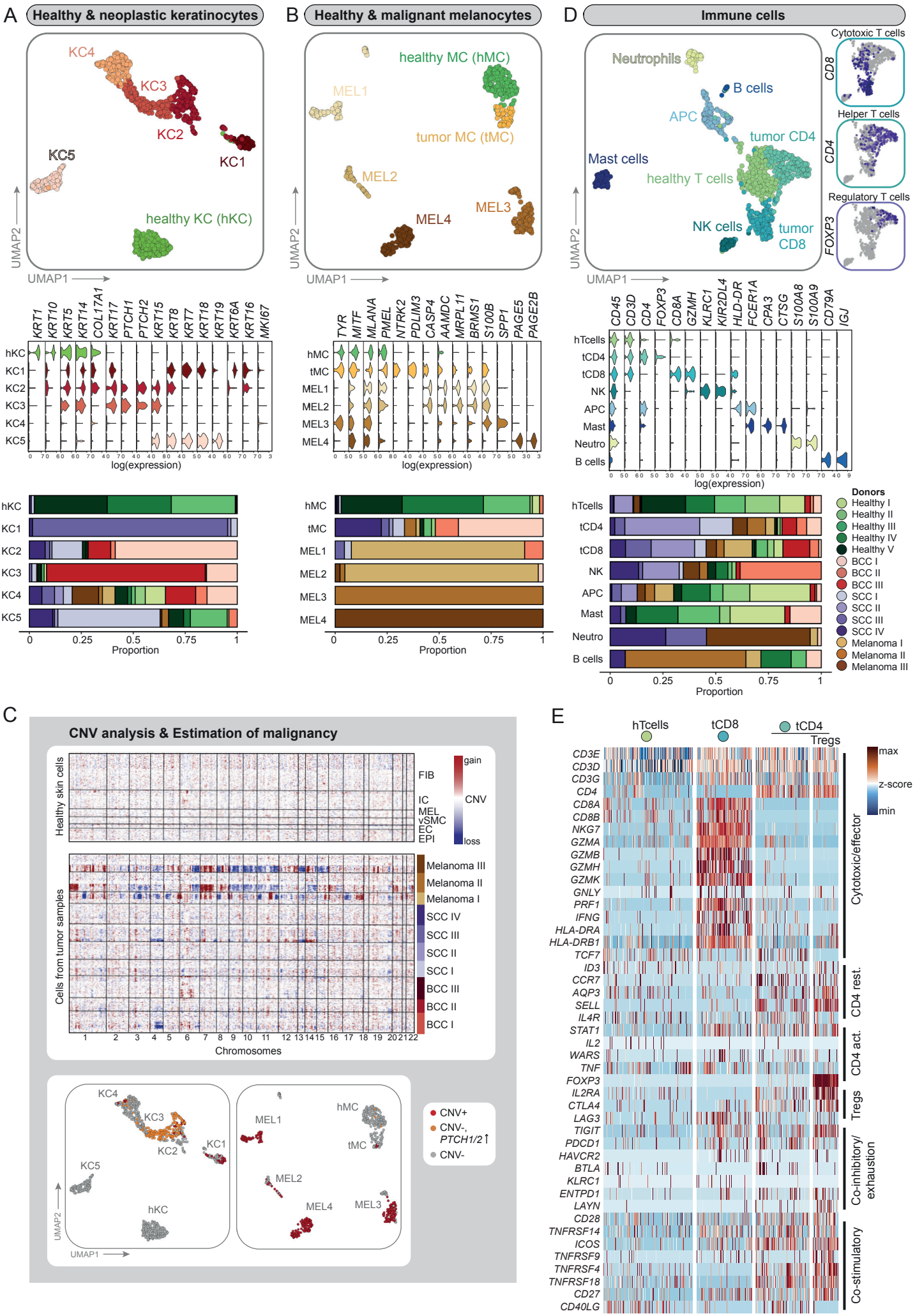
A
Healthy & neoplastic keratinocytes
KC4
KC3
KC2
KC1
KC5
healthy KC (hKC)
UMAP2
UMAP1
KRT1 KRT10 KRT5 KRT14 COL17A1 KRT17 PTCH1 PTCH2 KRT15 KRT8 KRT7 KRT18 KRT19 KRT6A KRT16 MKI67
hKC KC1 KC2 KC3 KC4 KC5
log(expression)
hKC KC1 KC2 KC3 KC4 KC5
0 0.25 0.5 0.75 1
Proportion
B
Healthy & malignant melanocytes
healthy MC (hMC)
MEL1
tumor MC (tMC)
MEL2
MEL3
MEL4
UMAP2
UMAP1
TYR MITF MLANA PMEL NTRK2 PDLIM3 CASP4 AAMDC MRPL11 BRMS1 S100B SPP1 PAGE5 PAGE2B
hMC tMC MEL1 MEL2 MEL3 MEL4
log(expression)
hMC tMC MEL1 MEL2 MEL3 MEL4
0 0.25 0.5 0.75 1
Proportion
D
Immune cells
Neutrophils
B cells
APC
tumor CD4
Mast cells
healthy T cells
NK cells
tumor CD8
UMAP2
UMAP1
Cytotoxic T cells
CD8
Helper T cells
CD4
Regulatory T cells
FOXP3
CD45 CD3D CD4 FOXP3 CD8A GZMH KLRC1 KIR2DL4 HLD-DR FCER1A CPA3 CTSG S100A8 S100A9 CD79A IGJ
hTcells tCD4 tCD8 NK APC Mast Neutro B cells
log(expression)
hTcells tCD4 tCD8 NK APC Mast Neutro B cells
0 0.25 0.5 0.75 1
Proportion
Donors
Healthy I
Healthy II
Healthy III
Healthy IV
Healthy V
BCC I
BCC II
BCC III
SCC I
SCC II
SCC III
SCC IV
Melanoma I
Melanoma II
Melanoma III
C
CNV analysis & Estimation of malignancy
Healthy skin cells
FIB
IC
MEL
vSMC
EC
EPI
gain
CNV
loss
Cells from tumor samples
Melanoma III
Melanoma II
Melanoma I
SCC IV
SCC III
SCC II
SCC I
BCC III
BCC II
BCC I
1 2 3 4 5 6 7 8 9 10 11 12 13 14 15 16 17 18 19 20 21 22
Chromosomes
KC4
KC3
KC2
KC1
KC5
hKC
UMAP2
UMAP1
MEL1
hMC
tMC
MEL2
MEL4
MEL3
CNV+
CNV-, PTCH1/2↑
CNV-
E
hTcells
tCD8
tCD4
Tregs
max
z-score
min
CD3E
CD3D
CD3G
CD4
CD8A
CD8B
NKG7
GZMA
GZMB
GZMH
GZMK
GNLY
PRF1
IFNG
HLA-DRA
HLA-DRB1
TCF7
ID3
CCR7
AQP3
SELL
IL4R
STAT1
IL2
WARS
TNF
FOXP3
IL2RA
CTLA4
LAG3
TIGIT
PDCD1
HAVCR2
BTLA
KLRC1
ENTPD1
LAYN
CD28
TNFRSF14
ICOS
TNFRSF9
TNFRSF4
TNFRSF18
CD27
CD40LG
Cytotoxic/effector
CD4 rest.
CD4 act.
Tregs
Co-inhibitory/ exhaustion
Co-stimulatory

Figure 3

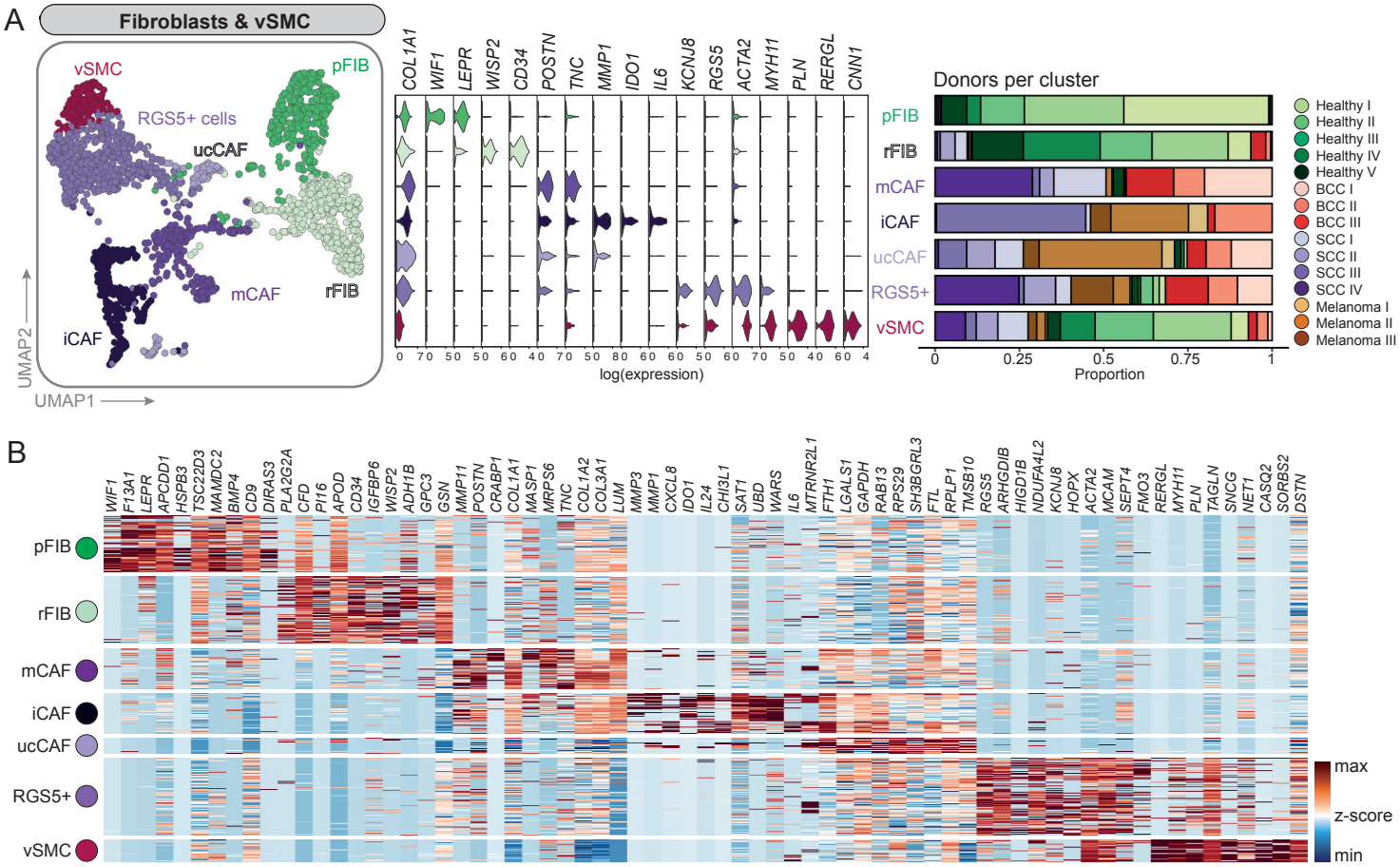
A
Fibroblasts & vSMC
vSMC
pFIB
RGS5+ cells
ucCAF
mCAF
rFIB
iCAF
UMAP2
UMAP1
COL1A1
WIF1
LEPR
WISP2
CD34
POSTN
TNC
MMP1
IDO1
IL6
KCNJ8
RGS5
ACTA2
MYH11
PLN
RERGL
CNN1
log(expression)
Donors per cluster
pFIB
rFIB
mCAF
iCAF
ucCAF
RGS5+
vSMC
Proportion
Healthy I
Healthy II
Healthy III
Healthy IV
Healthy V
BCC I
BCC II
BCC III
SCC I
SCC II
SCC III
SCC IV
Melanoma I
Melanoma II
Melanoma III
B
max
z-score
min

Figure 4

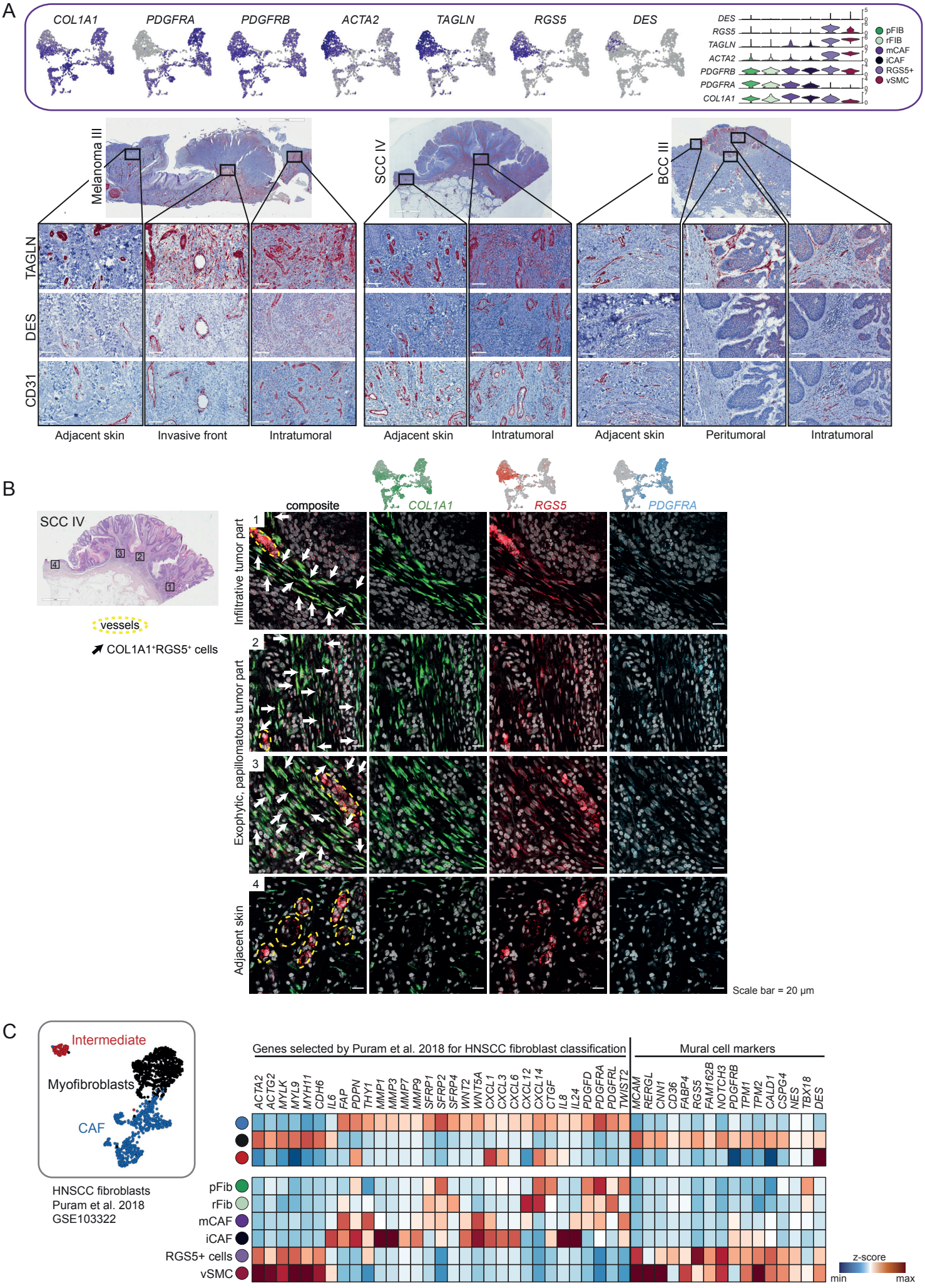
A
COL1A1
PDGFRA
PDGFRB
ACTA2
TAGLN
RGS5
DES
pFIB
rFIB
mCAF
iCAF
RGS5+
vSMC
Melanoma III
SCC IV
BCC III
TAGLN
DES
CD31
Adjacent skin
Invasive front
Intratumoral
Adjacent skin
Intratumoral
Adjacent skin
Peritumoral
Intratumoral
B
SCC IV
vessels
COL1A1+RGS5+ cells
composite
COL1A1
RGS5
PDGFRA
Infiltrative tumor part
Exophytic, papillomatous tumor part
Adjacent skin
Scale bar = 20 µm
C
Intermediate
Myofibroblasts
CAF
HNSCC fibroblasts
Puram et al. 2018
GSE103322
Genes selected by Puram et al. 2018 for HNSCC fibroblast classification
Mural cell markers
ACTA2 ACTG2 MYLK MYL9 MYH11 CDH6 IL6 FAP PDPN THY1 MMP1 MMP3 MMP7 MMP9 SFRP1 SFRP2 SFRP4 WNT2 WNT5A CXCL1 CXCL3 CXCL6 CXCL12 CXCL14 CTGF IL8 IL24 PDGFD PDGFRA PDGFRL TWIST2
MCAM RERGL CNN1 CD36 FABP4 RGS5 FAM162B NOTCH3 PDGFRB TPM1 TPM2 CALD1 CSPG4 NES TBX18 DES
pFib
rFib
mCAF
iCAF
RGS5+ cells
vSMC
z-score
min
max

Figure 5

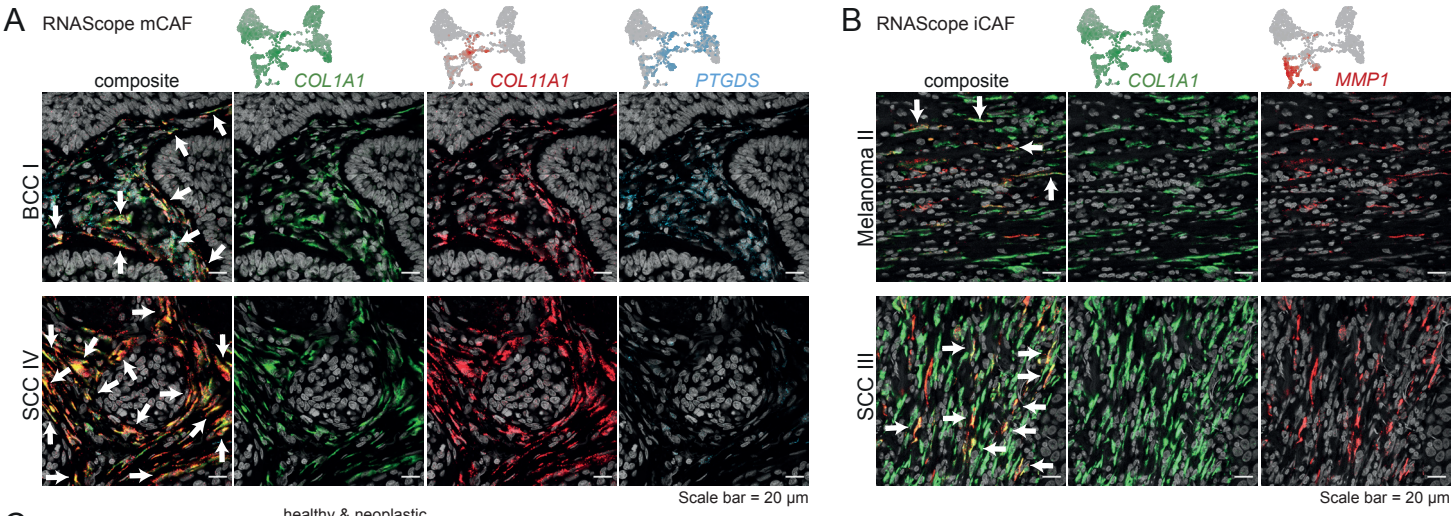
A
RNAScope mCAF
composite
COL1A1
COL11A1
PTGDS
BCC I
SCC IV
Scale bar = 20 µm
B
RNAScope iCAF
composite
COL1A1
MMP1
Melanoma II
SCC III
Scale bar = 20 µm

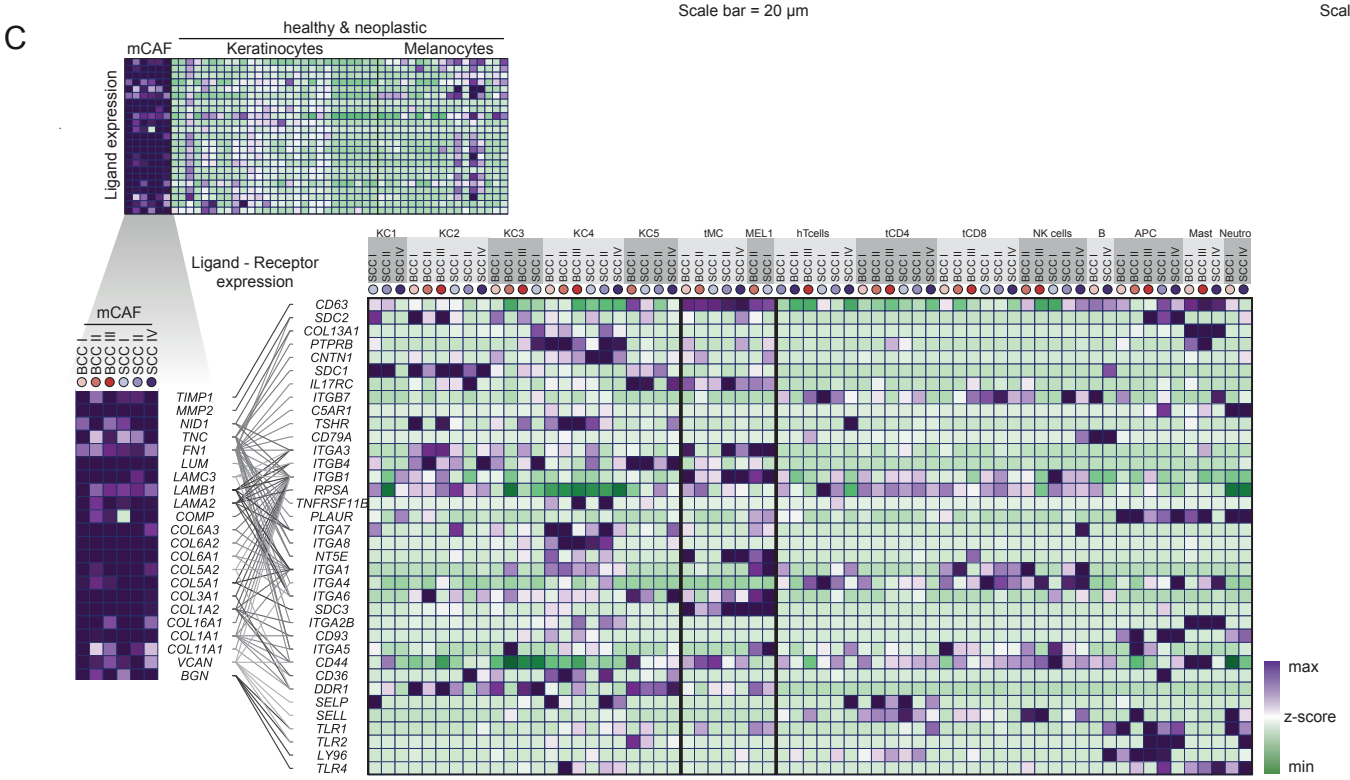
C
healthy & neoplastic
mCAF
Keratinocytes
Melanocytes
Ligand expression
Ligand - Receptor expression
mCAF
BCC I
BCC II
BCC III
SCC I
SCC II
SCC IV
TIMP1
MMP2
NID1
TNC
FN1
LUM
LAMC3
LAMB1
LAMA2
COMP
COL6A3
COL6A2
COL6A1
COL5A2
COL5A1
COL3A1
COL1A2
COL16A1
COL1A1
COL11A1
VCAN
BGN
CD63
SDC2
COL13A1
PTPRB
CNTN1
SDC1
IL17RC
ITGB7
C5AR1
TSHR
CD79A
ITGA3
ITGB4
ITGB1
RPSA
TNFRSF11B
PLAUR
ITGA7
ITGA8
NT5E
ITGA1
ITGA4
ITGA6
SDC3
ITGA2B
CD93
ITGA5
CD44
CD36
DDR1
SELP
SELL
TLR1
TLR2
LY96
TLR4
KC1
KC2
KC3
KC4
KC5
tMC
MEL1
hTcells
tCD4
tCD8
NK cells
B
APC
Mast
Neutro
max
z-score
min

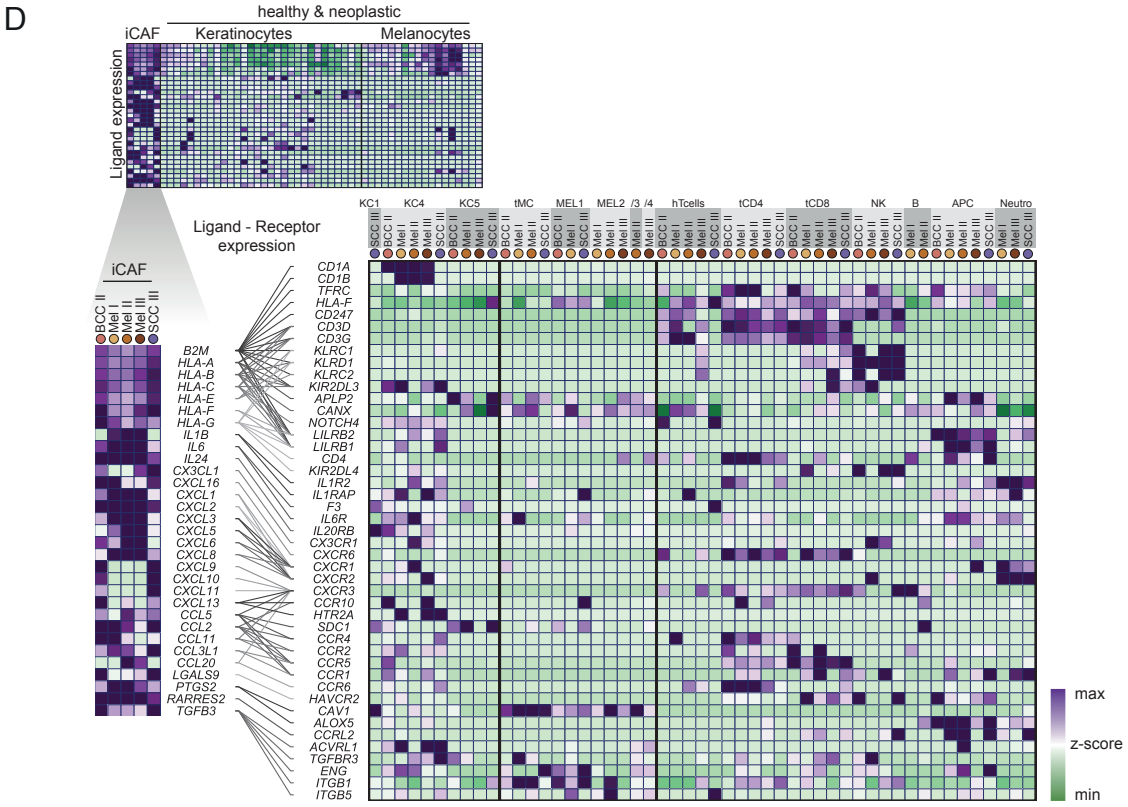
D
healthy & neoplastic
iCAF
Keratinocytes
Melanocytes
Ligand expression
Ligand - Receptor expression
iCAF
BCC II
Mel I
Mel II
Mel III
SCC III
B2M
HLA-A
HLA-B
HLA-C
HLA-E
HLA-F
HLA-G
IL1B
IL6
IL24
CX3CL1
CXCL16
CXCL1
CXCL2
CXCL3
CXCL5
CXCL6
CXCL8
CXCL9
CXCL10
CXCL11
CXCL13
CCL5
CCL2
CCL11
CCL3L1
CCL20
LGALS9
PTGS2
RARRES2
TGFB3
CD1A
CD1B
TFRC
HLA-F
CD247
CD3D
CD3G
KLRC1
KLRD1
KLRC2
KIR2DL3
APLP2
CANX
NOTCH4
LILRB2
LILRB1
CD4
KIR2DL4
IL1R2
IL1RAP
F3
IL6R
IL20RB
CX3CR1
CXCR6
CXCR1
CXCR2
CXCR3
CCR10
HTR2A
SDC1
CCR4
CCR2
CCR5
CCR1
CCR6
HAVCR2
CAV1
ALOX5
CCRL2
ACVRL1
TGFBR3
ENG
ITGB1
ITGB5
KC1
KC4
KC5
tMC
MEL1
MEL2 /3 /4
hTcells
tCD4
tCD8
NK
B
APC
Neutro
max
z-score
min

Figure 6

A *in situ* cytokine expression of CAFs

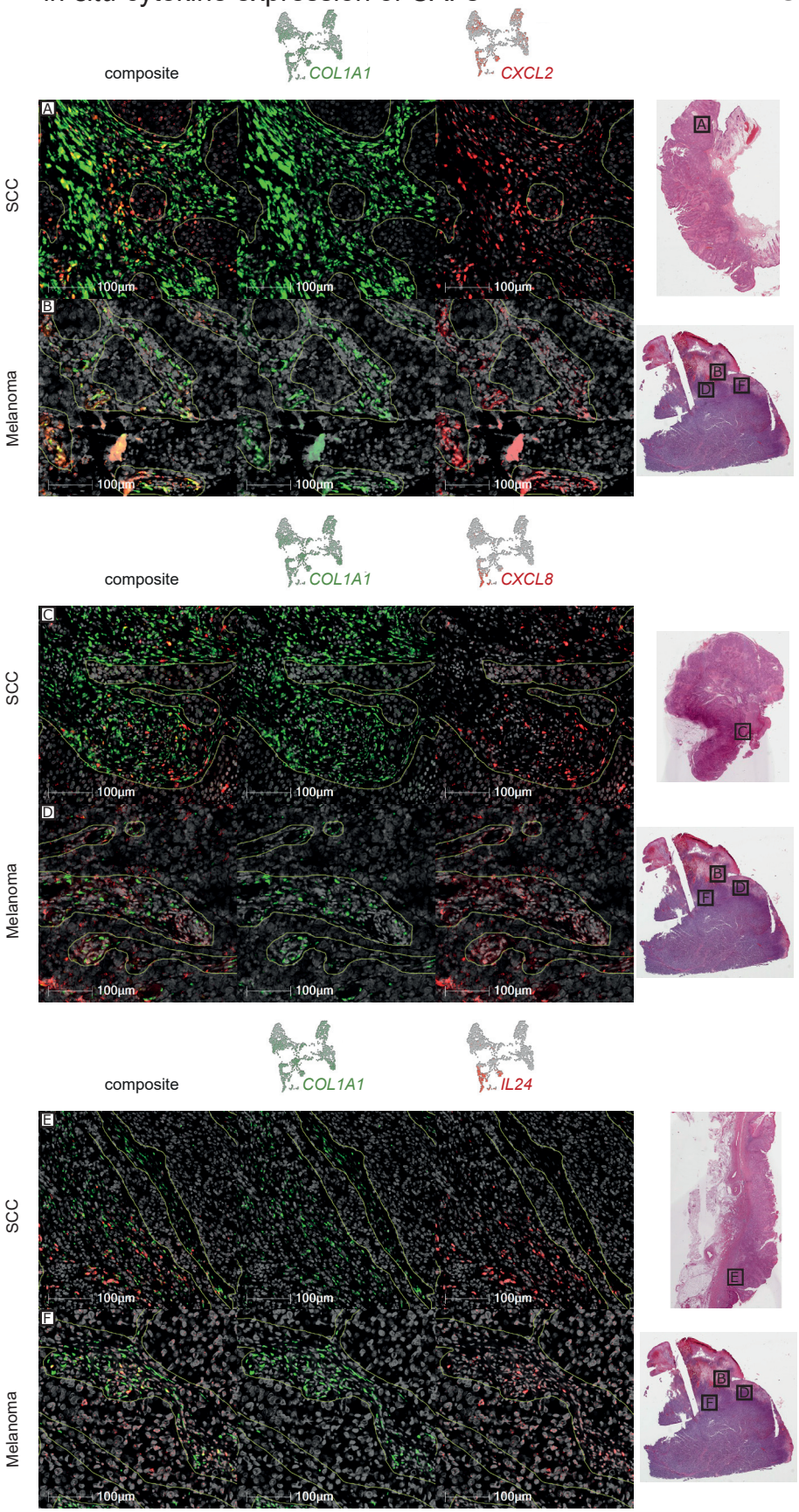

C *in vitro* cytokine expression of NHDFs and skin cancer cells

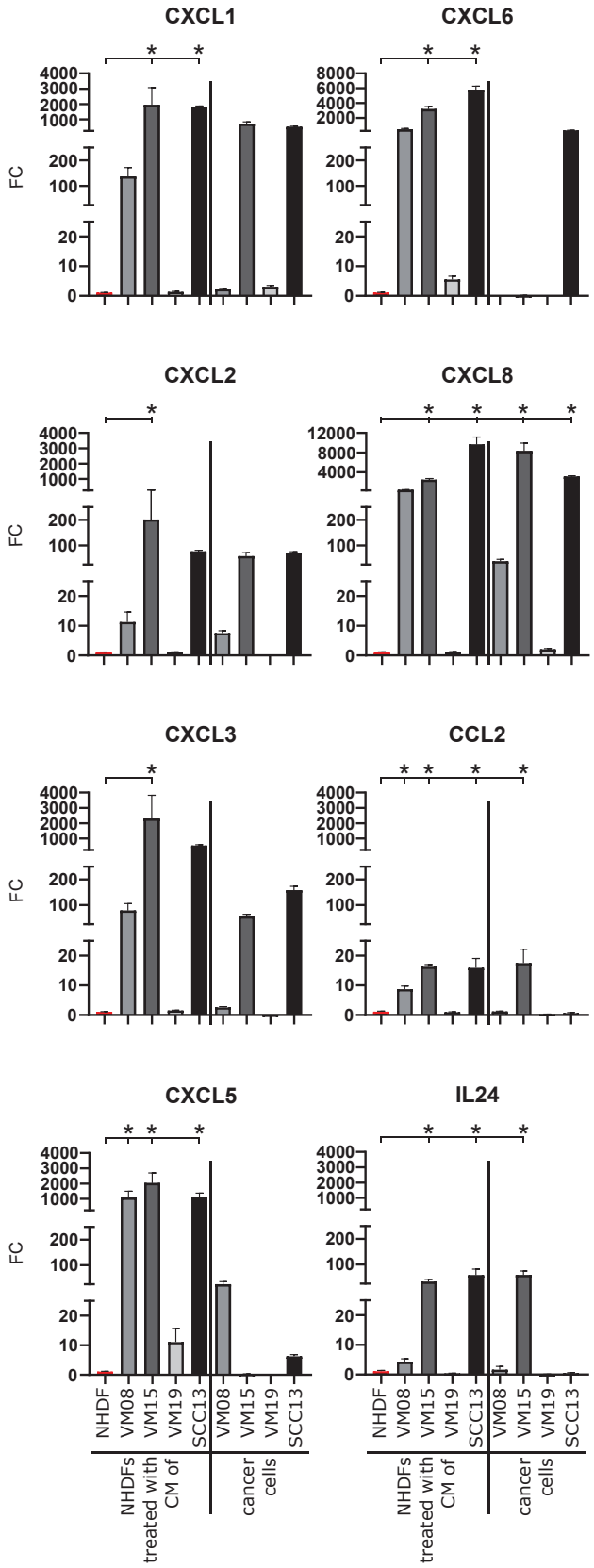

B *in situ* quantification of cytokine expressing CAFs

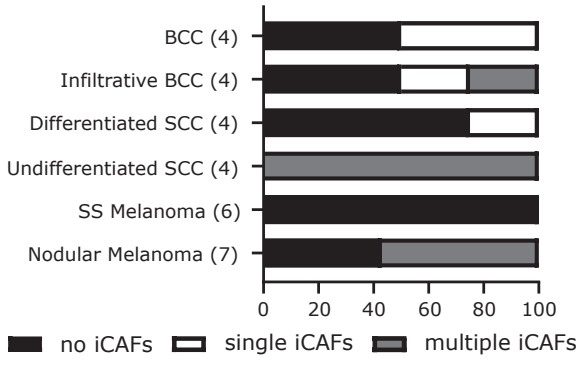
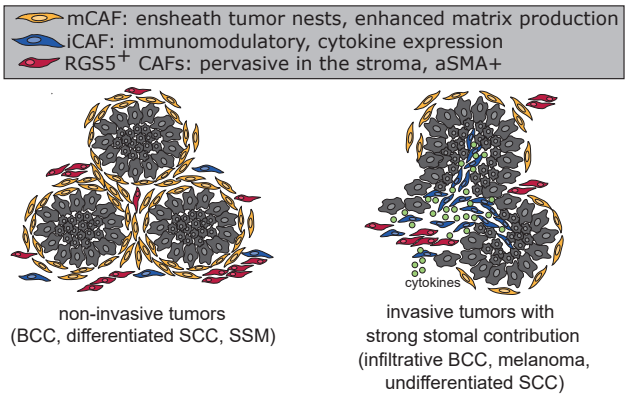
D